1. Theory and Characteristics of the Mössbauer Effect

1.1 Theory of the Mössbauer Effect

As discussed in the preface, Mössbauer spectroscopy is now used routinely as an analytical tool in many different areas of science. However, its introduction is relatively recent compared to many other spectroscopies. Why did it take so long for the Mössbauer effect to be discovered? The main reason is that resonant emission and absorption are much more difficult to achieve with gamma rays than with optical photons because of the much higher energies of gamma rays. The law of conservation of momentum requires that a free nucleus emitting a photon must recoil just as a rifle recoils on emitting a bullet. The recoil energy, E_R, is given by

$$E_R = E_\gamma^2 / 2Mc^2 \tag{1.1}$$

where E_γ is the energy of the gamma ray, M is the mass of the emitting nucleus and c is the velocity of light. For ^{57}Fe, the recoil energy is 0.0020 eV (3.2×10^{-22} J) compared to1.0×10^{-10} eV for the yellow sodium D lines.

To see the importance of this for resonant emission and absorption we need to compare this recoil energy with the natural linewidth of the emission line. This is defined by the Heisenberg uncertainty principle which sets a limit on how accurately we can simultaneously measure two complementary variables. In this case the two complementary quantities are the uncertainties in energy and time, ΔE and Δt respectively, such that

$$\Delta E \, \Delta t \geq \hbar \tag{1.2}$$

where $\hbar$ is Planck's constant divided by 2π. The time uncertainty, Δt, is interpreted as the mean life, τ, of the level emitting the gamma ray and is related to the more familiar half life, $T_{½}$, by $\tau = T_{½}/\ln 2$.

For ^{57}Fe, the half life of the 14.4 keV level is 97.7 ns which gives the uncertainty in the energy as 4.67×10^{-9} eV. This uncertainty becomes the natural linewidth, Γ, of the transition where

$$\Gamma = \hbar/\tau \tag{1.3}$$

and this sets the best resolution which can be obtained when utilising the entire time spectrum of the gammas. Electromagnetic theory then tells us that the intensity, I(E), of the emission line as a function of energy, E, will have the Lorentzian shape given by

$$I(E) = \frac{(\Gamma/2)^2}{(E-E_0)^2+(\Gamma/2)^2} \tag{1.4}$$

where E_0 is the centre of the emission line. This shape is depicted in Figure 1.1 where it can be seen that Γ is the full width of the line at half maximum (FWHM).

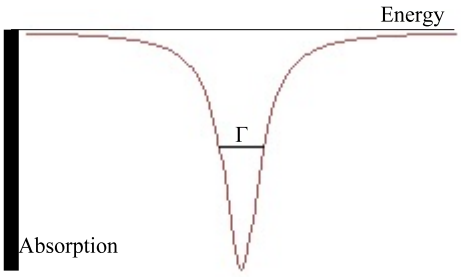

Figure 1.1. The Lorentzian (or Breit-Wigner) line shape. The Full Width at Half Maximum (FWHM), Γ, is normally used to define the spread of energies.

We can now see that although the recoil energy for ^{57}Fe seemed small when compared to the total energy of the gamma (1.4×10^{-7}), it is some 4.3×10^5 times larger than the linewidth, so that the energy of the emitted gamma is shifted to lower energies by the equivalent of 4.3×10^5 linewidths. There is consequently little chance of it being reabsorbed by another ^{57}Fe nucleus, with the situation being made worse by a factor of two because the absorbing nucleus will need additional energy to compensate for its recoil which will be in the opposite direction. This is shown schematically in Figure 1.2.

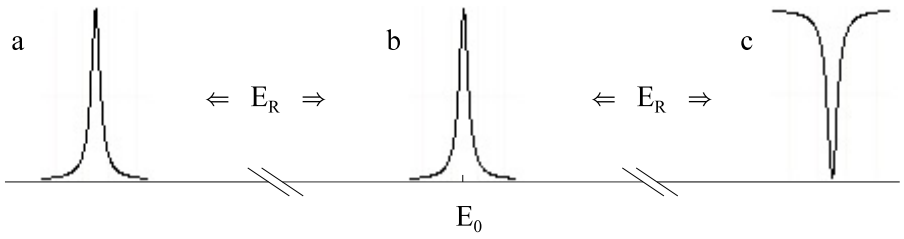

Figure 1.2. Illustration of the shift in the energy of the gamma ray from the nuclear transition energy E_0 at (b) to the free atom recoil value at (a), while a free atom absorber will require that the energy be at (c).

Mössbauer's discovery was that if we deal with nuclei in a solid, rather than free nuclei as described above then, in some fraction of cases, the gamma will be emitted without recoil and will have the proper energy E_0 of the transition. This does not imply some breakdown of the law on conservation of momentum but rather that, in these recoilless transitions, the momentum is taken up by the solid as a whole. If we take the common pestle and mortar preparation for powdered samples, then the mass of a typical particle is approximately 10^7

times the mass of a single nucleus and the loss of energy is reduced by this factor to an unmeasurably small value.

1.1.1 Recoilless Fraction

One of the most important parameters for defining the usefulness of a Mössbauer transition is the fraction of gammas which are emitted and absorbed without recoil. If this is too low, then the counting times needed to obtain an acceptable spectrum become prohibitively long.

The recoilless fraction, or f-value as it is commonly called, is given by

$$f = \langle \exp [-i\mathbf{k}.\mathbf{x}] \rangle^2 \quad (1.5)$$

where **k** is the wave vector of the gamma ray ($|\mathbf{k}| = 2\pi/\lambda$) and **x** is the vector displacement of the emitting nucleus (or atom). The average, denoted by the angular brackets, must be taken over the lifetime of the nucleus. For most solids at moderate temperatures, we can assume that the atomic vibrations may be modelled as a simple harmonic oscillator and then eq. 1.5 can be evaluated as

$$f = \exp [-k^2 \langle x^2 \rangle] \quad (1.6)$$

where $\langle x^2 \rangle$ is the root mean square amplitude of the vibration along the direction of the gamma emission.

This expression is known as the Lamb-Mössbauer factor and many readers will recognize it as the Debye-Waller factor which defines the intensity of diffracted X-ray and neutron beams. However, there is one important difference and this is the time average mentioned above. For X-ray and neutron diffraction, the average is taken over the scattering time ($\sim 10^{-14}$s), while for the Mössbauer effect the average must be taken over the nuclear lifetime (typically 10^{-7} s). For most purposes, this distinction is not important. However, for Mössbauer relaxation and scattering processes, and particularly for the use of the synchrotron radiation as discussed in section 2.4.6, this distinction is very important.

To proceed beyond the general form of eq. 1.6 we need more information about the frequency distribution of the atomic vibrations in the solid in which our Mössbauer nucleus is embedded. To take the spectrum for a particular mineral is too limiting, but one can take the Debye approximation to the frequency spectrum which assumes a distribution which is parabolic with frequency

$$G(f) = 3N f^2 / f_D^3$$

where the maximum frequency f_D is chosen so that the total number of frequency modes is 3 times the number of atoms, N, in the solid. This enables one to derive the following expression for the f-value as a function of the temperature, T

$$f = \exp\left[\frac{-6E_R}{k_B\theta_D}\left[\frac{1}{4}+\left(\frac{T}{\theta_D}\right)^2\int_0^{\theta_D/T}\frac{y\,dy}{e^y-1}\right]\right] \quad (1.7)$$

where k_B is the Boltzmann constant, θ_D is the so-called Debye temperature. This somewhat unwieldy expression can be integrated numerically to produce a plot of f against T for different values of θ_D. as shown in Figure 1.3. It can be seen that the f-value does not reach unity, even at T = 0, because quantum mechanics tells us that there are still some lattice vibrations, the so-called zero-point vibrations, at this temperature. It is notable how rapidly the f-value drops for materials with weaker bonding (lower Debye temperature) although this is rarely the case with mineral samples. However, hydrous materials such as peat and lignite can have very small f-values at room temperature and then have a large increase at or somewhat below 0°C. This is due to a change in the Debye temperature as the water content freezes and hence no single curve in Figure 1.3 is appropriate at high and low temperatures. We will return to Figure 1.3 when we consider the quantitative measurement of site populations, ferrous/ferric ratios and phase proportions in section 1.7.4, where the relative difference in f-value for two sites or materials with different Debye temperatures is very important.

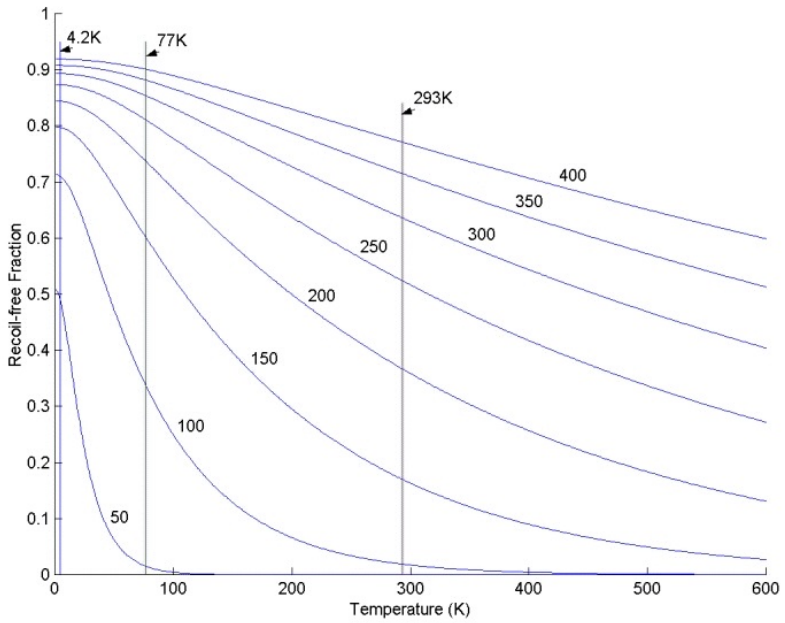

Figure 1.3. Calculated f-values for ^{57}Fe, based on the Debye model, as a function of temperature, for Debye temperatures of the material as indicated (F. Ninio).

The Debye temperature acts as a convenient parameter to characterize the strength of the atomic bonding. However, we must remember that it was introduced merely as a normalising parameter in a mathematical expression and so is not a true physical constant of our mineral comparable with measurable entities such as the velocity of sound or the bulk modulus. Nevertheless, many measurable quantities can be parameterized in terms of the Debye temperature, for example, the low-temperature specific heat. Each of these quantities is some different average over the assumed parabolic frequency spectrum, so it should not be surprising that they all yield slightly different values for θ_D. In particular, at low temperatures, only the low frequency part of the spectrum is thermally populated, and a parabolic distribution is quite accurately representative of the true frequency spectrum as would be measured, for example, by neutron scattering. However, the Lamb-Mössbauer factor takes in contributions over the higher frequency modes, including optical modes which do not even appear in the model Debye spectrum. Since the population of these modes is a function of temperature, then the average over them will change with sample temperature so that a Debye temperature derived from the Lamb-Mössbauer factor will depend on the temperature range over which the spectra were measured.

Thus this characteristic "Debye temperature" is in fact a function of temperature itself and this limitation must be borne in mind when utilising it to compare the areas of Mössbauer spectra taken at different temperatures. Nevertheless, the parameter is useful in many contexts as long as its limitations are borne in mind.

Rather than utilising the integral expression in eq. 1.7 there are two convenient asymptotic expressions which are appropriate at low and high temperatures. These are

$$f = \exp\left[\frac{-E_R}{k_B\theta_D}\left(\frac{3}{2}+\frac{\pi^2\theta_D^2}{T^2}\right)\right], \tag{1.8}$$

if $T \leq 0.3\ \theta_D$,

and

$$f = \exp\left[\frac{-6E_RT}{k_B\theta_D^2}\right] \tag{1.9}$$

if $T \geq 0.5\ \theta_D$.

We can see from eq. 1.8 that the limiting value of f at T = 0 is

$$f = \exp\left[\frac{-3E_R}{2k_B\theta_D}\right] \tag{1.10}$$

The preceding discussion is important for understanding the problems which can arise in trying to determine quantitatively the proportions of different phases from the areas of their subspectra when the spectra are taken at different

temperatures. Each different phase (mineral) will have its particular f-value and these f-values will have a different temperature dependence. Thus the area ratio of two phases can change considerably in spectra taken at different temperatures, none of which may be the true phase ratio.

An important example of the effect of the difference in f-values for iron atoms in different sites in the same material is provided by the spinels and garnets. If we consider magnetite, Fe_3O_4, the tetrahedral or A sites are occupied by Fe^{3+} ions while the octahedral or B sites are occupied by iron ions which, at room temperature, undergo dynamic electron hopping between Fe^{2+} and Fe^{3+}, giving an average valency of $Fe^{2.5+}$. Thus we can write the formula as $(Fe^{3+})[Fe^{2+}\ Fe^{3+}]O_4$, and hence expect that the area of the subspectrum due to the B sites should be twice that of the A site contribution. However, this is not the case because the ratio f_B/f_A is 0.94(2) at room temperature (Sawatsky *et al.* 1969) rising to 0.99(1) at T = 0 with effective Debye temperatures of $\theta_D(A) = 334(10)$ K and $\theta_D(B) = 314(10)$ K. An extension of this argument suggests that when magnetite is cooled below the Verwey transition of 120 K and the electron hopping ceases (see section 5.2), then we would expect that the f-value would now be different for each of the different iron sites, but we are not aware that anyone has attempted to measure this since even the fitting of these spectra is the subject of argument in the literature (see Section 5.2). Also, in terms of our description using a Debye temperature, the fact that the two sites have different Debye temperatures emphasizes that the Debye temperature is not a uniquely definable parameter of the material.

There are three variants from this general picture which should be pointed out. The first is that we have assumed that the emitting nucleus is embedded in a macroscopic solid. However, it is clear conceptually that as the size of the particles in the solid decreases, then somewhere before we get down to single atoms, it will become energetically possible for the entire particle to recoil. The criterion for this is usually taken as being when the recoil energy (Equation 1.1) is equal to the linewidth (Equation 1.3) and for ^{57}Fe this gives a diameter of 10.6 nm. The appropriate mean square displacement for substituting into Equation 1.b then becomes

$$\langle x^2 \rangle = \langle x_A^2 \rangle + \langle x_P^2 \rangle$$

where $\langle x_A^2 \rangle$ is the mean square displacement of the atom with respect to the particle and $\langle x_P^2 \rangle$ is the mean square displacement of the particle with respect to the laboratory.

The second variant concerns the applicability of the Debye model, particularly in predicting the temperature dependence. The model of the lattice vibrations assumes that the atoms vibrate in a parabolic potential. However, there are some cases where this is not applicable: examples include atoms in cage materials (zeolites, clathrates), in very anisotropic materials (graphite), in light van der Waals solids (solid Ne, H_2, He), $FeCl_2$, ThO_2:Fe, and soft mode

materials such as many ferro- and antiferroelectrics (*e.g.* $M^{2+}TiO_3$ and related materials) (see for example Kolk 1984).

The third variant is that the f-value for an impurity atom in a lattice will not be the same as for one of the host atoms because of the different bonding possible and the size difference of the atoms. If the impurity atom has an appreciably different mass, then its vibrational frequency spectrum will be different from that of the host atom. If the impurity mass is much less than that of the host, then it undergoes high frequency vibrations which are very localized near the impurity because they are above the allowed frequency modes which can propagate in the host. If the impurity atom has a much heavier mass, then it will undergo low frequency quasi-localized vibrations.

1.1.2 Requirements for a Mössbauer Nuclide

One of the questions which colleagues have often raised is "Why can't you do a Mössbauer spectrum of x?" where x is an element in which they have a particular interest. We are now in a position to be able to see what are the requirements in order to be able to observe the Mössbauer effect.

The maximum value of the recoilless fraction is given by eq. 1.10 and it can be seen to require a small value of the ratio of E_R/θ_D. The value of E_R (eq. 1.1) is determined by the nuclear properties and since the nuclear masses only change by about an order of magnitude from Z = 12 to the heaviest nuclei, then the dominant effect is the energy of the gamma ray, which appears as the squared power. The result is that transmission geometry spectra can only be taken for gamma rays with energy, $E_\gamma \leq 100$ keV, and up to 150 keV for scattering geometry. This is a severe limitation, since a large proportion of gamma-ray energies are in the MeV region.

The energy of the gamma ray sets another limitation - the temperature range over which experiments may be carried out. If we look at eq. 1.6, since k is proportional to E_γ, then for the higher gamma ray energies we must keep $\langle x^2 \rangle$ small to compensate, which means reducing the temperature. Thus experiments using many transitions must be carried out below about 50K in order to obtain a measurable absorption.

A second requirement is that this low energy gamma ray must be a transition to the ground state, otherwise we will not be able to make up an absorber which is able to absorb the incoming gamma ray.

This satisfies the criteria for being able to observe the Mössbauer effect, but this does not necessarily make it useful. For it to be useful, the resolution must be adequate to be able to observe the various hyperfine interactions and hence deduce the associated electronic properties. As discussed in section 1.1, the resolution is defined by the linewidth and since the hyperfine interactions are typically of order 10^{-9} to 10^{-6} eV, this sets an upper value on the linewidth. Eq.

1.2 enables us to convert this to a restriction on the excited state nuclear lifetime which must be of order nanoseconds or greater.

Typical nuclear lifetimes are $<10^{-12}$ s and it is only relatively rare nuclear structures which will give lifetimes to fit our requirements.

In order to carry out conventional Mössbauer experiments, it is also necessary to have a radioactive source. This requires a parent nuclide which will feed the desired transition and has a conveniently long half life - preferably many months to years. ^{57}Co is the parent for the ^{57}Fe transition and has a half-life of 270 d. The decay scheme of ^{57}Co to ^{57}Fe is shown in Figure 1.4.

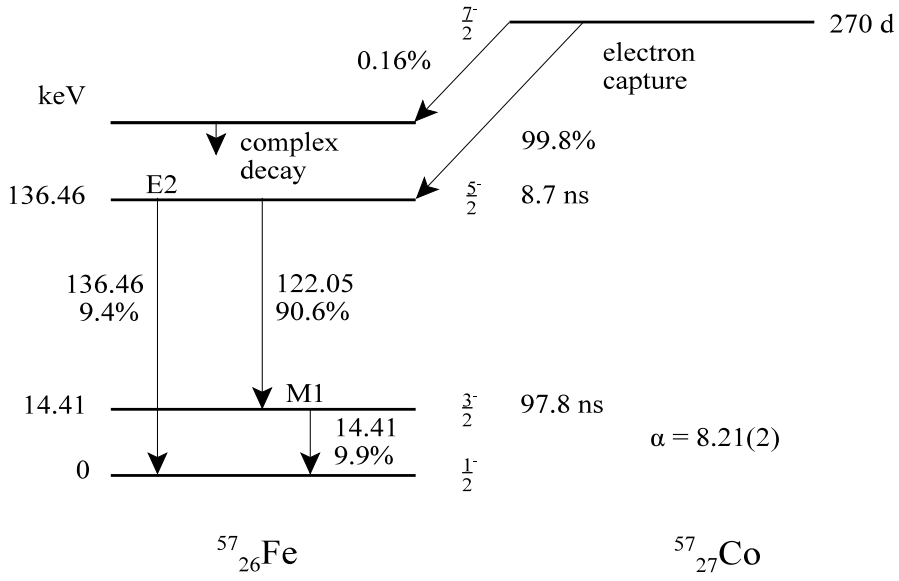

Figure 1.4. The decay scheme of ^{57}Co to ^{57}Fe.

It will be noticed in Figure 1.4 that there is a severe loss of intensity in going from the 122 keV transition (91%) to the 14.4 keV transition(9.9%). This is because the 14.4 keV level has a probability of emitting an internal conversion electron which is 8.2 times larger than the probability of emitting a gamma ray (Johnson 1970). This is very unfortunate from the standpoint of transmission Mössbauer experiments because only 10% of the ^{57}Co decays produce useful gammas, but it does have the trade-off in making conversion electron Mössbauer spectroscopy (CEMS) a viable method of studying surfaces.

In order to study natural materials it is also desirable that the resonant nuclide should be reasonably abundant. In the case of iron, the Mössbauer isotope, ^{57}Fe, only constitutes 2.14% of the total, but the other characteristics are

so favourable, that this is adequate. Nevertheless, isotopically enriched iron can be useful when studying, for example, surface deposition or dilute impurities.

Thus we have seen that there are several restrictions which have to be satisfied in order to have a good Mössbauer transition. Unfortunately, although there are many good transitions, there are also very significant gaps in the periodic table where there are no suitable Mössbauer nuclides. In particular, the nuclear levels are such that the little used nuclide ^{40}K is the only useful nuclide lighter than ^{57}Fe. It is a fortunate accident for many branches of science that an isotope of iron turned out to be the most convenient Mössbauer nuclide.

There are only approximately eight Mössbauer transitions which can be carried out at room temperature. These are ^{57}Fe (14.4 keV), ^{119}Sn (23.8 keV), ^{121}Sb (37.1 keV), ^{125}Te (35.5 keV) although here the absorber is actually radioactive too, ^{129}I (27.7 keV), ^{151}Eu (21.6 keV), ^{155}Dy (25.6 keV), ^{169}Tm (8.4 keV) and ^{181}Ta (6.2 keV). All the remaining higher energy transitions require low temperatures. The members of the above list will also show improved spectra at low temperatures and in many cases these may be necessary, particularly for organic compounds.

The Mössbauer periodic table is shown in Figure 1.5. Apart from Fe, the most common transitions used on geological samples are ^{119}Sn, ^{121}Sb, ^{151}Eu and ^{197}Au. There are some nuclides which do not have a parent with a convenient half-life and it is likely that these will become accessible in the near future through the use of synchrotron radiation. The main one of potential geological interest is ^{61}Ni.

Tables of the Mössbauer transitions may be found in the following books in the bibliography: Greenwood and Gibb (1971), Gütlich *et al.* (1978), Kolk (1984), Vertes and Nagy (1990).

There is one other aspect of the resolution of the Mössbauer effect which deserves mention. This is the ratio of E_γ/Γ which equates to the Q-factor of the resonance, a term commonly used for electrical and mechanical resonators. Typical values for these range from 10-10^3 for mechanical systems and over 10^6 for a cooled maser. For ^{57}Fe, (using the experimental value of 2Γ) the Q-factor is 1.55×10^{12} and for ^{67}Zn is 1.9×10^{15}. This superb fractional energy resolution is why the Mössbauer effect was able to be used to carry out the only earthbound test of Einstein's theory of special relativity.

1.2 Magnetism

A Mössbauer spectrum is essentially a microscopic magnetization measurement because each emission or absorption of a gamma gives information on the magnetic state of the atom concerned. So a basic knowledge of magnetism is essential for understanding the Mössbauer spectra of many materials. This includes an understanding of their behaviour in magnetic fields, which are

H																He
Li	Be											B	C	N	O	F	Ne
Na	Mg											Al	Si	P	S	Cl	Ar
K 40 29.4 0.012	Ca	Sc	Ti	V	Cr	**Mn** 55 125.9 100	**Fe** 57 14.4 2.17	Co	**Ni** 61 67.4 1.13	Cu	**Zn** 67 93.3 4.11	Ga	**Ge** 73 13.3 7.8	As	Se	Br	**Kr** 83 9.3 11.55
Rb	Sr	Y	Zr	Nb	Mo	**Tc** 99 140.5 0	**Ru** 99 89.4 12.7	Rh	Pd	**Ag** 1.9 158.4 48.16	Cd	In	**Sn** 119 23.9 8.58	**Sb** 121 37.2 57.25	**Te** 125 35.5 7.14	**I** 129 27.8 0	**Xe** 129 39.6 26.44
Cs 133 81.0 100	**Ba** 133 12.3 0	**La** 139 166.0 99.91	**Hf** 178 93.2	**Ta** 181 6.23 99.99	**W** 183 46.5 14.3	**Re** 187 134.2 62.6	**Os** 189 36.3 16.1	**Ir** 193 73.0 62.7	**Pt** 195 98.8 33.8	**Au** 197 77.4 100	**Hg** 199 158.4 16.84	Tl	Pb	Bi	Po	At	Rn
Fr	Ra	Ac															

No usable transition

Only observable at low temperatures

Can be observed at room temperature

Ce	**Pr**	**Nd**	**Pm**	**Sm**	**Eu**	**Gd**	**Tb**	**Dy**	**Ho**	**Er**	**Tm**	**Yb**	**Lu**
	141	145	147	149	151	155	159	161	165	166	169	170	175
	145.2	72.5	91.0	22.5	21.6	86.5	58.0	25.6	94.7	80.6	8.42	84.3	113.8
	100	8.30	0	13.8	47.8	14.8	100	18.88	100	33.6	100	3.05	97.41
Th	**Pa**	**U**	**Np**	**Pu**	**Am**	Cm	Bk	Cf	Es	Fm	Md	No	Lr
232	231	238	237	240	243								
49.8	84.2	44.7	59.5	42.9	84.0								
100	0	99.27	0	0	0								

Figure 1.5. Periodic table showing the most commonly used Mössbauer transition for each of the elements. The three numbers with the elements are the mass number, the gamma ray energy in keV and the isotopic abundance of the selected nuclide. Note that some elements have more than one useful transition with, for example, ^{129}I being favoured over ^{131}I because of its better nuclear properties although the former does not exist naturally and so such absorbers are radioactive. Natural minerals containing iodine would need to use ^{131}I. (Adapted from Mössbauer Effect Reference and Data Journal **23**, 180 (2000)).

frequently used to elucidate interpretations or improve resolution. It is very difficult to interpret and understand microscopic measurements unless one already has an understanding of the likely macroscopic situation.

All atoms and ions are either diamagnetic or paramagnetic. All materials with a sufficient concentration of paramagnetic species will eventually become magnetically ordered through magnetic exchange or dipole-dipole interactions if cooled to a sufficiently low temperature, even if this temperature needs to be μK or less. Some materials are already magnetically ordered at room temperature and have to be heated before they become paramagnetic.

When one thinks of magnetically ordered materials, iron is usually the first element which comes to mind. However, iron is unusual in that it can also be diamagnetic. Some examples are pyrite, FeS_2, the ferrocyanides and in materials such as the superconducting rare earth iron silicides (Cashion *et al.* 1980).

1.2.1 Diamagnetic Materials

Diamagnetic materials have no magnetic moment on the atom and are repelled from a magnet. Common Mössbauer nuclides in this category are tin and gold. In the presence of a magnetic field, a magnetic moment is induced on these atoms and, as required by Lenz's law, it is in the opposite direction to the applied field.

Fitting the Mössbauer spectrum of a diamagnetic material in an externally applied field should show that the field on the nucleus is the same as the applied field. Potassium ferrocyanide is sometimes used to calibrate high field magnets this way since it is difficult to calibrate magnets above 10 T using, for example, NMR or the Hall effect. The measured magnetic field at the nucleus will be positive - the significance of which will become clearer when we discuss magnetic **hyperfine** fields in more detail.

1.2.2 Paramagnetic Materials

Nearly all iron minerals are paramagnetic at room temperature, the few common exceptions being pyrite, which is diamagnetic, and hematite, magnetite, maghemite, goethite, and native iron. The latter materials are magnetically ordered, and heating them above their magnetic ordering temperature will turn them into paramagnets, but they will order magnetically again on cooling. Note that in fine particle or aluminium substituted minerals, particularly goethite, they can be superparamagnetic (see Section 1.4.2) and hence produce a spectrum which appears to be from a paramagnet.

Paramagnetic atoms have a magnetic moment, but these fluctuate

continually so that the vector sum of all the magnetic moments is zero. Applying a magnetic field to a paramagnet causes the fluctuations to decrease and produce a net magnetization in the direction of the magnetic field. The increase of magnetization with field usually approximately follows the Brillouin function appropriate to the spin of the atom. At a sufficiently high magnetic field, all the moments will be aligned and the material is said to be magnetically saturated. The Brillouin curve is a function of B/T, where B is the applied magnetic field and T is the absolute temperature, so that a larger magnetization can be obtained by increasing the field or by lowering the temperature.

1.2.3 Magnetically Ordered Materials

The principal classes of magnetically ordered materials are ferromagnets, antiferromagnets and ferrimagnets. In dealing with them, it is convenient to consider ferrimagnets with antiferromagnets when discussing their ordering, but to put them with ferromagnets when discussing the effect of magnetic fields. The section concludes with a brief discussion of magnetic frustration and the types of ordering in materials which do not have long range order.

1.2.3.1 Ferromagnets

The common understanding of a "magnet" as a material in which the magnetic moments on all the atoms are aligned in the one direction, really describes a ferromagnet (Figure 1.6a). This alignment is caused by a positive exchange interaction between (principally) nearest neighbour magnetic moments, which causes the direction of the moment on one atom to influence the directions of the moments of its neighbours. When the sum of the energy of these interactions with its neighbours becomes comparable to the thermal energy, k_BT, where k_B is the Boltzmann constant and T is the absolute temperature, then the material becomes magnetically ordered and this ordering temperature is called the Curie temperature, T_C.

The information on the direction of the moments, which is carried by the exchange interaction, is passed between the magnetic atoms by one of two methods. In insulators, the orbitals of intervening atoms, for example the p-orbitals of oxygen, have their spins polarized by the, so-called, superexchange interaction. Since the lobes of a p-orbital are on opposite sides of the atom, this mechanism works best when the metal-oxygen-metal bonding angle is approximately 180°.

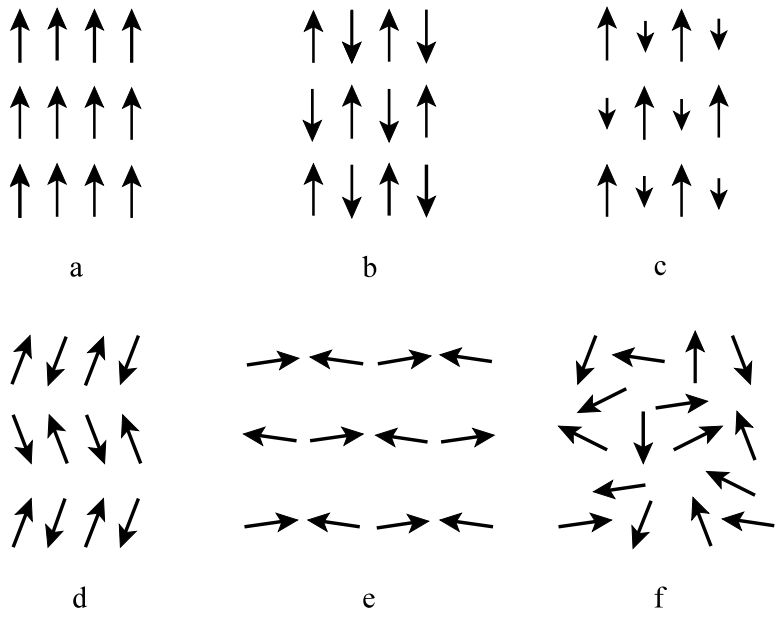

Figure 1.6. Schematic diagram of the arrangement of magnetic moments on adjacent magnetic atoms for (a) a ferromagnet, (b) an antiferromagnet, (c) a ferrimagnet, (d) a canted antiferromagnet, (e) a weak ferromagnet and (f) a speromagnet.

An important consideration in minerals is the effect of small local changes in the composition on the magnetic properties. One example is the replacement of some of the magnetic atoms, *e.g.* Fe^{3+}, by another element, such as the diamagnetic Al^{3+}, or by vacancies. This puts gaps in the superexchange links and reduces the sum of all the magnetic interactions, hence causing a reduction in the ordering temperature which is initially linear with the proportion of impurity atoms. If the proportion of magnetic atoms which are replaced becomes too large, then it may no longer be possible for the magnetic information to be transmitted through the material and it will no longer order even at T = 0. This critical concentration is known as the percolation limit. Its numerical value depends on the number of near magnetic neighbours and hence is determined by the crystal structure.

In metals, the spins of the conduction electrons are polarized by the atomic moments and they carry the information about the magnetic interactions through the material.

The ferromagnets which we have considered were assumed to have all their moments pointing in the same direction, known as a collinear

ferromagnet. However, there are more complicated types of ferromagnets, such as helical ferromagnets which occur commonly in the rare earth metals, and canted ferromagnets, in which the moments on neighbouring atoms are at some definite angle to each other, but there is one direction along which there is a non-zero moment. The reader is unlikely to encounter these in mineralogical applications so we shall not deal with them here. Further details can be found in most texts on magnetism.

1.2.3.2 Antiferromagnets and Ferrimagnets

The exchange interaction is not always positive. A negative interaction is antiferromagnetic and leads to an ordering which favours antiparallel alignment of magnetic moments (Figure 1.6b) below the ordering temperature known as the Néel temperature. Although this diagram shows (in two dimensions) that the nearest neighbours of an atom all have antiparallel magnetic moments, this is not always the case. In some structures, *e.g.* fcc, it is not possible to have an arrangement in which each atom has all twelve neighbours aligned antiparallel. In others, it is energetically more favourable to have lines or sheets of atoms which are aligned parallel, but which are antiparallel to the neighbouring lines or sheets. But whatever the arrangement, the total number of moments pointing in each direction is the same so that the net magnetization for all the atoms must sum to zero.

So far we have considered materials which have only one type of magnetic atom. However, if there are two (or more) types which are arranged in a crystallographically ordered way on different lattice sites, then an antiferromagnetic alignment will not lead to complete cancellation (Figure 1.6c). These materials are called ferrimagnets and in the form of ferrites are responsible for a considerable part of the magnetics industry. The majority of magnetic recording is based on the spinel-structured, maghemite, γ-Fe_2O_3, and the ceramics for microwave applications, radio aerials and fridge magnets are based on the hexagonal barium or strontium ferrites or the cubic (Ni,Zn) or (Mn,Zn) spinel ferrites or yttrium iron garnet.

The perovskite structure, rare earth orthoferrites, $RFeO_3$, have the simple arrangement shown in Figure 1.6c. However, the spinels, AB_2O_4, are more complicated with three different exchange interactions, J_{AA}, J_{BB} and J_{AB}. The latter usually dominates and is antiferromagnetic. Using the nomenclature ( ) and [ ] for the tetrahedral and octahedral sites, we note that the inverse spinels, nickel ferrite, $(Fe^{3+})[Ni^{2+}Fe^{3+}]_2O_4$, and magnetite, $(Fe^{3+})[Fe^{2.5+}]_2O_4$, are both ferrimagnets due to the oppositely directed moments on the A and B sites. Magnesioferrite, $MgFe_2O_4$, has a nearly inverse structure with approximately 10% of the non-magnetic Mg atoms on the A sites, depending on the preparation, so that the oppositely-directed Fe moments on the A and B

sites do not completely cancel. However, the normal spinel, $(Zn)[Fe^{3+}]_2O_4$, has a non-magnetic A atom and is an antiferromagnet with the octahedral sites dividing themselves into two sublattices because of the antiferromagnetic J_{BB} interaction. With the wide variety of cations which can be accommodated in spinels, many complicated and also non-collinear arrangements can occur for different relative sizes of the three exchange interactions.

There are two modification of the antiferromagnetic structure in which the moments on different sublattices are no longer exactly antiparallel but are at some constant angle to each other. If the vector sum of the moments exactly cancel, as in Figure 1.6d, then this is known as a canted antiferromagnet. However, if the vector sum does not entirely cancel then this gives rise to a weak ferromagnet, as in Figure 1.6e, which has a net, small moment in the upwards direction. Hematite, α-Fe_2O_3, is the most common example of this.

1.2.3.3 Behaviour in Magnetic Fields

When a material becomes magnetically ordered, the magnetic moments have a preferred direction. For a collinear ferromagnet or ferrimagnet, this direction is called the "easy" direction. For many ferro- and ferrimagnets, this is a unique direction, for example, the symmetry axis in a hexagonal, tetragonal or trigonal crystal, with the directions at right angles to it being the "hard" directions. In cubic materials, for example α-Fe and Ni, the easy direction will be one of the <100>, <110> or <111> directions and in this case all of the equivalent directions of the family will be easy directions. The other two sets of directions are known as hard directions.

When applying a magnetic field so as to reverse the direction of magnetization, there is an anisotropy energy barrier which has to be overcome. If this barrier is small (<1000 A/m or 10 Oe), then the magnet is a soft magnet, such as α-Fe and many of its dilute alloys like FeSi, transition metal spinel ferrites, rare earth iron garnets, permalloy and amorphous metals. If the barrier is large (>10,000 A/m or 100 Oe), then the magnet is hard, for example the hexagonal alkaline earth ferrites, alnico or $Nd_2Fe_{14}B$.

The behaviour of **ferro-** and **ferrimagnets** in magnetic fields depends on the size of the anisotropy. An applied magnetic field larger than the anisotropy field will align all the moments with the applied field. However, one smaller than the anisotropy field will leave many of the moments pointing in different directions, although there will be an overall preference for alignment with the field. In a polycrystalline sample, crystallites with an easy axis near to the field direction will magnetize easily along the field. However, those with a hard direction nearest to the field direction, will require a larger field to get their magnetization to align. A sufficiently large field will achieve magnetic saturation, when all the moments are aligned along the field.

Application of a field in one direction, and then reversing it, causes the magnetization to describe a hysteresis loop and the value of the magnetization will tell how much alignment has been achieved.

These considerations become important in interpreting the Mössbauer spectra in applied magnetic fields because the observed field on a nucleus is the vector sum of the applied field and the hyperfine field, the latter being proportional to, and usually oppositely directed, to the magnetization on that atom.

The behaviour of **antiferromagnets** in a field also depends on the anisotropy, but even more markedly. Unlike the ferro- and ferrimagnets, there is now no net moment for the field to act on, so it must first break the antiferromagnetic coupling of some of the ions to achieve this.

For materials with anisotropy energy smaller than the exchange energy, which includes most Fe^{3+} compounds, there are two possibilities. Crystallites with their moments aligned along an easy axis near to the applied field direction will undergo a spin flop at some critical field, when the moments turn through a large angle so that they are now both typically 60-70° from the magnetic field direction, but with their components perpendicular to the field being oppositely aligned. This enables the two sublattices to remain approximately antiparallel, hence minimising the exchange energy at the expense of the smaller anisotropy energy. Crystallites with their moments at an appreciable angle to the applied field direction will have their moments smoothly rotate towards the field direction as the field increases. Both groups will eventually reach saturation, but it takes a larger field to saturate the second group. Thus, spectra taken in an applied field will, in general, have a considerable distribution of angles between the local magnetization and the field.

For antiferromagnets with an anisotropy energy much larger than the exchange energy, which includes most Fe^{2+} compounds, crystallites with their moment directions (easy axis) close to the applied field direction will undergo a spin flip at some critical field in which all the moments which were pointing the wrong way suddenly reverse their direction together and saturation is achieved almost immediately. Moments which are pointing more nearly perpendicular to the applied field will slowly rotate towards the field but this can require very large fields if the anisotropy is large. Secondly, many ions, particularly the rare earths (except for Gd^{3+}), have an anisotropic g-value, so that the moment on the atom actually decreases in magnitude as it rotates. This of course, decreases the energy gain of aligning the moments and there is no general solution to mathematically describe this situation. (The g-value is a tensor which describes the size of the magnetic moment of an ion along any direction relative to the crystal axes. It arises because of the different shapes of the magnetic d-orbitals, for the transition metal ions, or the f-orbitals, for

the rare earth ions, and the fact that some of the orbitals have lower energies in the crystal field, created by the surrounding ions, than other members of their set.)

1.2.3.4 Other Types of Ordering

There are two other types of ordering which readers should be aware of. The first type is really a group of types which can occur in crystallographically disordered materials. The principal one in this group is speromagnetism (Coey 1973), whose members include some of the poorly crystalline ferric oxyhydroxides. The magnetic moments of speromagnets are fixed in space, but their direction may have only limited correlation with the directions of their neighbours (Figure 1.6f). The magnetic coupling can be mixed ferro- and antiferromagnetic (depending on separation) or only antiferromagnetic and it is most likely to occur with either magnetic atoms or magnetic particles randomly distributed in a non-magnetic matrix. Other related types of ordering include sperimagnetism, asperomagnetism, etc. and the detailed review by Hurd (1982) or any recent book on magnetic materials will provide more information.

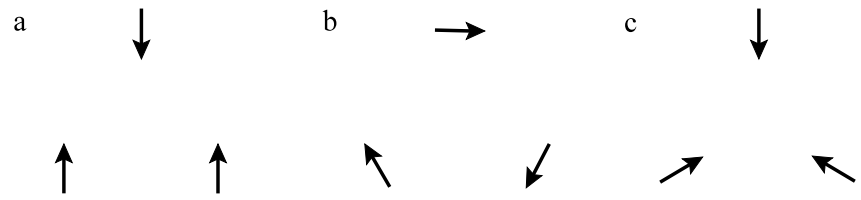

Figure 1.7. Diagram of a triangular array of magnetic moments showing three possible moment configurations, none of which enable a simple antiferromagnetic interaction between each pair to be satisfied.

The second type of behaviour is perhaps better described as a "non-ordering" and is called magnetic frustration. This can occur under a variety of situations in which the set of antiferromagnetic interactions between the magnetic atoms cannot be satisfied simultaneously. A simple example is to consider a lattice in which the magnetic atoms occur at the apices of an equilateral triangle. This is very similar to the extended situation in many clay minerals. If we call the three atoms A, B and C, we can see that, for example, if the moment on atom A points up (Figure 1.7a), then the antiferromagnetic interaction with each of B and C would like them to both point down. However, this does not satisfy the antiferromagnetic interaction between B and C. Other possible frustrated arrangements are shown in Figure 1.7b,c. This

frustration is sufficient to prevent magnetic ordering even though the magnetic interactions may be quite strong. Sometimes, very small distortions or the effects of next nearest neighbours can break the impasse.

1.3 Hyperfine Interactions

The electron-nucleus interactions were first observed in optical spectra as smaller splittings than the previously observed "fine structure" (which are due to electron-electron interactions) and hence were dubbed hyperfine splittings. However, while they may be "hyperfine" in importance as viewed from the electrons, they are very important when viewed from the nucleus.

The most important electron-nucleus interaction is the Coulomb interaction which binds the electrons to the nucleus. This is not considered to be a hyperfine interaction as it is approximately 10^{10} times as strong as the true hyperfine interactions.

The three hyperfine interactions of importance here are the isomer shift, the electric quadrupole interaction and the magnetic dipole interaction. We shall deal with each in turn, and also treat the thermal or second order Doppler shift together with the isomer shift since the two effects produce the same change to the spectra. In describing the interactions, we have tried to concentrate on creating a sound physical understanding rather than a mathematical derivation as we believe that this will be more useful to most of our readers.

1.3.1 Isomer (or Chemical) Shift

The first hyperfine interaction, the isomer shift, is really a correction to the coulomb term mentioned above. The origin of the "isomer" name is historical and is now probably somewhat anachronistic. However, there are two good reasons to avoid the occasionally used name of "chemical shift". The first is to avoid confusion with the related NMR parameter of the same name. The second is that the term "isomer shift" is usually used to include the thermal shift and chemical effects, although some researchers use the term "centre shift" for this line movement due to the two effects jointly. Consequently, if one wants a term to cover the purely chemical effects associated with bonding, etc., then we believe that, at this stage in our history, it would be better to develop a new name since the name chemical shift has often been used without explicitly removing the temperature shift. We shall deal with the thermal, or second order Doppler, shift in the next section. Note that the letters "CS" have been used by some authors to denote the chemical shift and by others to denote the centre shift.

The Coulomb interaction assumes that the electrons move around the nucleus at a sufficiently large distance that the nucleus can be considered as a point charge. However, the nucleus has a finite size, with a radius of approximately

$$R = 1.2 \times 10^{-15} Z^{1/3} \text{ m}$$

where Z is the atomic number.

While most of the electron charge density is at distances large compared with this, particularly the bonding electrons which dominate our thoughts in dealing with the chemistry and most other forms of spectroscopy, the s-electrons and the $p_{½}$-electrons have a small but finite probability of being inside the nucleus. This effect is dominated by the 1s electrons and has the effect of shifting the energies of all the nuclear levels.

This effect, by itself, would be unobservable because the shift is much smaller than our ability to either measure or predict theoretically these energies. However, in the course of emitting a gamma ray, the nucleus undergoes a transition from an excited state to a lower state and the radius of the nucleus is different in these two levels. The interaction in each level is the integration of the product of the nuclear charge density and the electron charge density over the region of overlap. Since the volume of the overlap region is different for the two nuclear states, the shift of each nuclear level is different as shown in Figure 1.8. This difference between the shifts is effectively a measure of the electron density in the very thin annular shell which makes up the difference in volumes of the two nuclear states.

This, principally s-, electron density will change in accord with the bonding of the atom and hence will, in principle, be different for every compound which the atom can be part of. Let us consider what these changes may be. If we start with a free atom, then incorporation in a solid may involve the atom becoming an ion or adopting metallic bonding. These result in the exchange of one or more electrons with its surroundings. If the electron is an s-electron, then it is clear that a change in s-electron density will eventuate. However, if a valency change involves, say, a d-electron, as in changing from Fe^{2+} to Fe^{3+}, then this electron was helping to shield the nuclear charge from the outer electrons and so the remaining electron charge cloud moves slightly inwards, thus producing a change in the s-electron density in the critical annular shell. This movement is best demonstrated when one contrasts the increased radii of anions from the free atom value with the decrease in radius on producing a cation.

More subtle changes are produced by bonding modifications which involve a change in coordination or covalency. Some of these changes were not necessarily predictable before isomer shift measurements were started. The first isomer shift measurement was by Kistner and Sunyar (1960) and the first quantitative description of the systematics was by Walker *et al.* (1961).

However, in order for us to understand the use of isomer shifts in studying mineral systems, it is more effective to correlate isomer shift variations within and between systems than to try and carry out first principles computation of the changes.

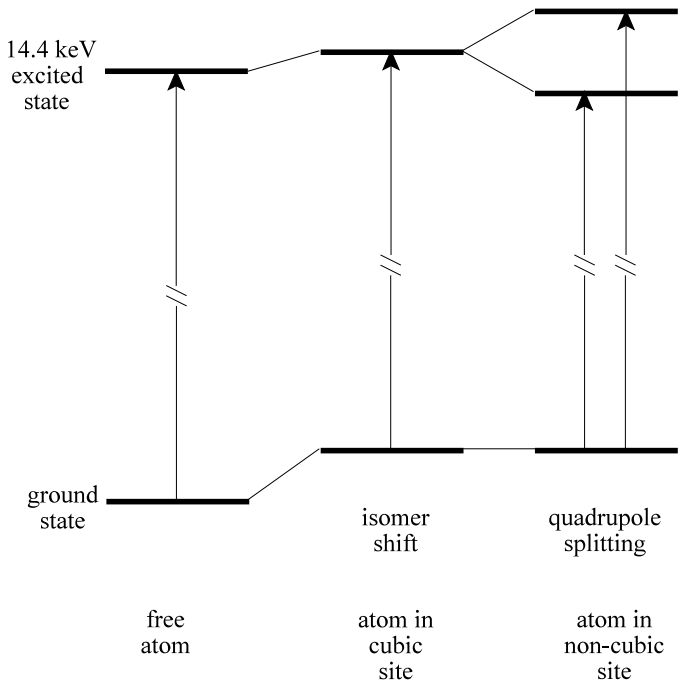

Figure 1.8. Energy level diagram for ^{57}Fe showing the change in the transition energy due to the isomer shift and the splitting of the excited state due to the quadrupole interaction. The diagram is also valid for other $^{3}/_{2} \rightarrow {}^{1}/_{2}$ transitions such as ^{119}Sn and ^{197}Au.

The mathematical expression for the isomer shift, δ, is given by

$$\delta = \frac{4\pi}{5} Ze^2 [|\Psi_a(0)|^2 - |\Psi_s(0)|^2] R \delta R$$

where $|\Psi(0)|^2$ is the relativistic electron density inside the nucleus at R = 0 for the absorber, a, and source, s, and δR is the thickness of the annular shell.

Thus we get a shift in the absorption line which is proportional to the difference in the electron density between the source and the absorber. The isomer shift is effectively a potential energy and most readers will recollect that the zero level of a potential energy is arbitrary and can be chosen to suit ourselves. Thus there is a reference chosen for each Mössbauer transition. For

^{57}Fe, the reference recommended by the Mössbauer Effect Data Center (Gettys and Stevens 1979) is α-iron at room temperature.

Before the references were firmly established, researchers made their own choice of convenient reference compounds. Readers searching through the literature will find several of these used and Table 1.1 gives the conversion for each of these to α-iron. Note the larger uncertainty in the stainless steel value due to the inherent range of nearest neighbour configurations for the iron atoms.

Table 1.1. Isomer shift conversion factors for ^{57}Fe (Stevens *et al.* 1998b, Silin *et al.* 1998). The number in the second column should be added to the quoted isomer shift with respect to a particular standard to convert it to the isomer shift relative to α-iron. The number in parentheses is the uncertainty in the last digit.

Reference material	Isomer shift of reference w.r.t. α-iron δ/Fe (mm/s)
Sodium nitroprusside (SNP) $Na_2Fe(CN)_5{\cdot}2H_2O$	-0.260(2)
Cr	-0.1473(3)
Stainless steel (usually 310)	-0.09(2)
Sodium ferrocyanide $Na_4Fe(CN)_6{\cdot}10H_2O$	-0.067(3)
Potassium ferrocyanide $K_4Fe(CN)_6{\cdot}3H_2O$	-0.035(7)
α-Fe	0
Rh	0.1090(3)
Pd	0.1684(2)
Cu	0.2268(5)
Pt	0.3437(6)

Conceptually, one may expect that the radius of the excited nuclear state will be larger than that of the ground state. This is usually true, but is not the case for ^{57}Fe. Thus an increasing isomer shift corresponds to a reduction in s-electron density.

1.3.1.1 Thermal Shift or Second Order Doppler Shift (SODS)

Changing the temperature of either the source or the absorber will alter the observed spectrum. There are two reasons for this. The first is that the solid state properties of the material may alter. Although the effect of thermal expansion is usually negligible, changes such as a crystallographic or magnetic phase transition, onset of superparamagnetism and so on may also occur. These changes are particular to the material and cannot be treated in a general fashion. However, all materials undergo a shift in the mean energy for emission or absorption of the gamma ray with change in temperature as was first measured and explained by Pound and Rebka (1960).

If we consider the effect of the atomic vibrations on the emission of the gamma ray then we can expand it in a power series of terms in (v/c), where v is the velocity of the atom and c is the velocity of light. Since the velocity along each of the three Cartesian axes is continually changing at a frequency of $>10^{12}$ Hz, the linear terms will average out to zero over the nuclear lifetime of approximately 100ns. However, the quadratic terms are always positive and so cannot average to zero. It was first realized by Josephson (1960) that when the gamma is emitted, the nucleus becomes lighter by $\delta m = E_\gamma/c^2$. Since a Mössbauer emission is recoilless, then the change in momentum, p, of the nucleus is zero. The total kinetic energy of the lattice changes by

$$\delta E = \delta\left(\frac{p^2}{2m}\right) = \frac{p^2}{2}\left(\frac{-\delta m}{m^2}\right) = \frac{v^2}{2c^2}E_\gamma .$$

Since δm is negative, the energy of the lattice increases and the energy of the gamma must decrease by the same amount.

Thus, an increase in temperature will result in an increase in v^2 and hence a decrease in the gamma energy. The same result holds for the absorption of a gamma by the absorber. The size of the energy shift depends inversely on the strength of the bonding since this determines the vibration amplitudes. However, for most mineral species, the bonding strengths are relatively similar and Table 1.2 gives the approximate shift which we may expect in the centroid of the ^{57}Fe spectrum of an absorber at different temperatures, compared to its position at room temperature. The assumed Debye temperature is approximately 350 K. At temperatures $\geq\theta_D$, the shift approaches the high temperature limit of

$$\delta(\text{SODS})/\delta T = -3k_B/2Mc = -7.29 \times 10^{-4}\ \text{mm/(s.K)}$$

for ^{57}Fe. A more complete evaluation may be found, for example, in Rancourt (1998), Figure 2. This shift may be used to estimate θ_D by fitting the

temperature dependence in the region $0.15 < T/\theta_D < 0.33$, where it is most sensitive.

Note that the Debye temperature evaluated from the thermal shift will not give the same value as that evaluated from the f-value. This is because the evaluation of $\langle x^2 \rangle$ from the frequency spectrum is weighted by $1/\omega$, where ω is the frequency, whereas the evaluation of $\langle v^2 \rangle$ is weighted by ω. Thus $\langle x^2 \rangle$ is weighted less by the higher frequencies. So we should expect to see greater discrepancies between θ_D values from the two measurements in compounds than in metals because of the presence of optical modes in the former. See section 1.1.1 for further comments on the Debye model.

Table 1.2. Approximate shift, relative to the value at room temperature, in the centroid of the Mössbauer spectrum of a typical iron-containing mineral at selected temperatures.

Temperature (K)	Approximate shift (mm/s)
600	-0.22
78	+0.12
4	+0.14

There is an interesting connection between this temperature shift of the energy and the "twin paradox" in Einstein's special theory of relativity. If a space traveller goes on a long journey and then returns to Earth, it is found that the traveller is younger than a twin who stayed behind. This is because the clock which is applicable to an entity travelling at speed, runs slower than a stationary clock and this effect has been confirmed for example, in measurements of the lifetimes of subatomic particles. In the case of the absorber, increasing the temperature causes the gamma ray's "clock" to run slower and the reduced frequency, f, corresponds to a reduction in energy, E, since they are related by $E = hf$, where h is Planck's constant. This provides a convenient memory aid in remembering which way the line will move with change in temperature.

1.3.2 Electric Quadrupole Hyperfine Interaction

When we were discussing the isomer shift we assumed that the nucleus was spherical in the ground and excited state. However any nucleus with an angular momentum, I, greater than ½ is allowed to be non-spherical and usually is. The measure of the deviation of the nuclear shape from being

spherical is called the nuclear quadrupole moment. It is defined mathematically as

$$Q = 1/e \int \rho(r) (3z^2 - r^2) dV$$

which assumes that the nuclear charge distribution, $\rho(r)$, is an ellipsoid of revolution around the z-axis and the integral extends over the nuclear volume. It can be seen that if the nucleus is prolate then $Q > 0$, while if it is oblate, then $Q < 0$.

The Mössbauer atom is surrounded by other atoms in its solid. This surrounding charge distribution can be described mathematically by a set of spherical harmonics in the same way as one describes the parameters in crystal field theory. If we limit the description to just the second order terms, this describes an ellipsoid, which correspond to the crystal field D and E terms.

It is conceptually easy to see that our ellipsoidal positively charged nucleus will have preferential and less preferred orientations inside this negatively charged crystal field ellipsoid. This results in a splitting of the nuclear levels, just as the D and E terms split the iron ion ground state levels. Since the nuclear ellipsoid looks the same if reversed across its equator, then the $|+m_I>$ and $|-m_I>$ levels remain degenerate.

The appropriate mathematical description of the crystal field ellipsoid is that it is the second derivative of the electric potential, in other words the electric field gradient (EFG). Any physically significant second order shape must have a set of three orthogonal principal axes, x, y and z such that we can describe the EFG by the three components

$$V_{xx} = \partial^2 V/\partial x^2, \qquad V_{yy} = \partial^2 V/\partial y^2, \qquad V_{zz} = \partial^2 V/\partial z^2.$$

However, since the electrostatic potential must satisfy Laplace's equation:

$$V_{xx} + V_{yy} + V_{zz} = 0,$$

this means that only two of these three parameters are independent. It is convenient to chose the axes so that

$$|V_{zz}| \geq |V_{xx}| \geq |V_{yy}|$$

and take the two independent parameters as V_{zz} and the asymmetry factor, η, which is defined as

$$\eta = (V_{xx} - V_{yy}) / V_{zz},$$

and hence must satisfy $0 \leq \eta \leq 1$.

The interaction between the nuclear electric quadrupole moment and the EFG is described by the Hamiltonian operator

$$\mathcal{H} = eQV_{zz}\frac{3I_z^2 - I(I+1) + \eta(I_x^2 - I_y^2)}{4I(2I-1)}$$

For ^{57}Fe, and other similar |3/2> to |1/2> transitions like ^{119}Sn and ^{197}Au, this Hamiltonian does not affect the ground state, since Q = 0, but splits the excited state into two levels separated by

$$\Delta = \tfrac{1}{2}eQ\,V_{zz}\sqrt{(1+\eta^2/3)}.$$

This splitting was first observed in ^{57}Fe by Kistner and Sunyar (1960). A nuclear level diagram is shown on Figure 1.8 for the situation before and after the EFG is introduced. Thus the EFG only partly lifts the (2I+1)-fold degeneracy of the nuclear levels. When $\eta = 0$, we see that Δ is half of the quadrupole coupling constant, $eQ\,V_{zz}$ ($\equiv e^2qQ$), from NQR. Note that there are inconsistencies in the literature as to whether e is taken as $\pm\ 1.6\times10^{-19}$ C, so that it is safer to quote either e^2qQ or q, but not eq or V_{zz}.

What can we say about the quantity V_{zz} and its relation to the solid which we are studying? So far, our description of V_{zz} is that of the EFG at the atomic site. If the solid was a pure ionic material, then we could calculate this EFG by doing a lattice sum over the surrounding ions. Although this worked well for the S-state rare earth ion Gd^{3+} (Barton and Cashion 1979) it is not sufficiently true for iron compounds, or any other Mössbauer nuclide, for it to be better than an approximation.

However, the nucleus sees this lattice EFG through the screen of its own electrons and this has the effect of modifying the EFG. To see the effect, we must treat the closed shell electrons and the valency electrons separately. The lattice EFG polarizes the closed shell electrons and this produces an enhanced EFG at the nucleus which can be written $(1 - \gamma_\infty)\,V_{zz}^{latt}$. The term γ_∞ is called the Sternheimer antishielding factor with the term antishielding implying that it amplifies the effect of V_{zz}^{latt}. This is a very large effect, with γ_∞ having values of up to -100 in the heavier atoms. A more exact method is to calculate the EFG at the nucleus directly with a program such as Wien 2k.

The valence electrons also contribute large EFGs. Table 1.3 gives the contributions of the p- and d- electrons to the EFG, where the term $\langle r^{-3}\rangle$ indicates the average value of r^{-3} for the electrons described. It can be seen that the sum of the EFG's for a closed shell of p- or d-electrons is zero. However, for example, for iron in the presence of a crystal field, the relative populations of the five d-electron wave functions can be very different, giving rise to a large EFG contribution.

This valency EFG also polarizes the core electrons to produce an EFG at the nucleus of $(1 - R_Q)\, V_{zz}^{val}$. The term R_Q has typical values of 0.2 - 0.3 and the electron-electron repulsion between the valency and core electrons causes it to reduce the valency EFG.

Thus the total EFG at the nucleus is given by

$$V_{zz}^{total} = (1 - \gamma_\infty)\, V_{xx}^{latt} + (1 - R_Q)\, V_{zz}^{val}.$$

It is instructive to consider how these contributions behave in ferric and ferrous compounds. High spin Fe^{3+} is an S-state ion so, even though the d-shell is not perfectly spherically symmetric, there is only a small EFG contribution from it. Consequently, high spin ferric ions have relatively small quadrupole splittings, typically 0.3-0.7 mm/s, although they can be double this latter value. High spin ferrous ions will have a large contribution from the 6^{th} d-electron and this gives typical splittings of 1.5-3.0 mm/s with a maximum of over 4 mm/s. In the low spin states, these splittings are reduced and it is significant that the standard single line absorber is the low spin compound potassium ferrocyanide. The strong CN^- ligands produce a perfectly octahedral environment to ensure that V_{xx}^{latt} is zero and drive the ferrous ion into a perfect low spin state. It can be seen from Table 1.3 that having two electrons in each of the d_{xy}, d_{yz}, and d_{zx} states will give a zero V_{zz}^{val} so both contributions are eliminated.

Table 1.3. The EFG contributions of p- and d-electrons

Electron state	V_{zz}^{val}.
p_x	$+(2/5) \langle r^{-3} \rangle_p$
p_y	$+(2/5) \langle r^{-3} \rangle_p$
p_z	$-(4/5) \langle r^{-3} \rangle_p$
d_{xy}	$+(4/7) \langle r^{-3} \rangle_d$
d_{yz}	$-(2/7) \langle r^{-3} \rangle_d$
d_{zx}	$-(2/7) \langle r^{-3} \rangle_d$
$d_{x^2-y^2}$	$+(4/7) \langle r^{-3} \rangle_d$
d_{z^2}	$-(4/7) \langle r^{-3} \rangle_d$

In a situation of mixed ligands, it is sometimes possible to add up the contributions of each ligand. This concept of the "partial quadrupole splitting" is due to Bancroft (Bancroft and Platt 1972, Bancroft *et al.* 1972, Bancroft 1973) and works if the metal-ligand bond distance is approximately constant and the contribution of the crystal field splitting to the EFG is negligibly small. Thus it is appropriate for filled or half-filled shells (Fe^{II}, Fe^{3+}) or main group elements with empty s and p shells (Sn^{IV}, Sb^{V}).

Knowledge of the crystal structure will often give some information about the directions of the EFG principal axes. If there is a unique axis of 3-, 4- or 6-fold symmetry through the Mössbauer atom site, then this must be the direction of V_{zz} and also η must be zero. Similarly, if the Mössbauer atom lies on a mirror plane, then one principal axis must be perpendicular to it.

A spectrum of the unsplit line of dilute iron in palladium and the quadrupole split spectrum of the garnet almandine, $Al_2O_3 \cdot 3FeO \cdot 3SiO_2$, are shown in Figure 1.9a, b which correspond to the two parts of Figure 1.8. The line positions for a quadrupole-split doublet are given by $\delta \pm \frac{1}{2}\Delta$, where δ is the isomer shift and Δ is the quadrupole splitting.

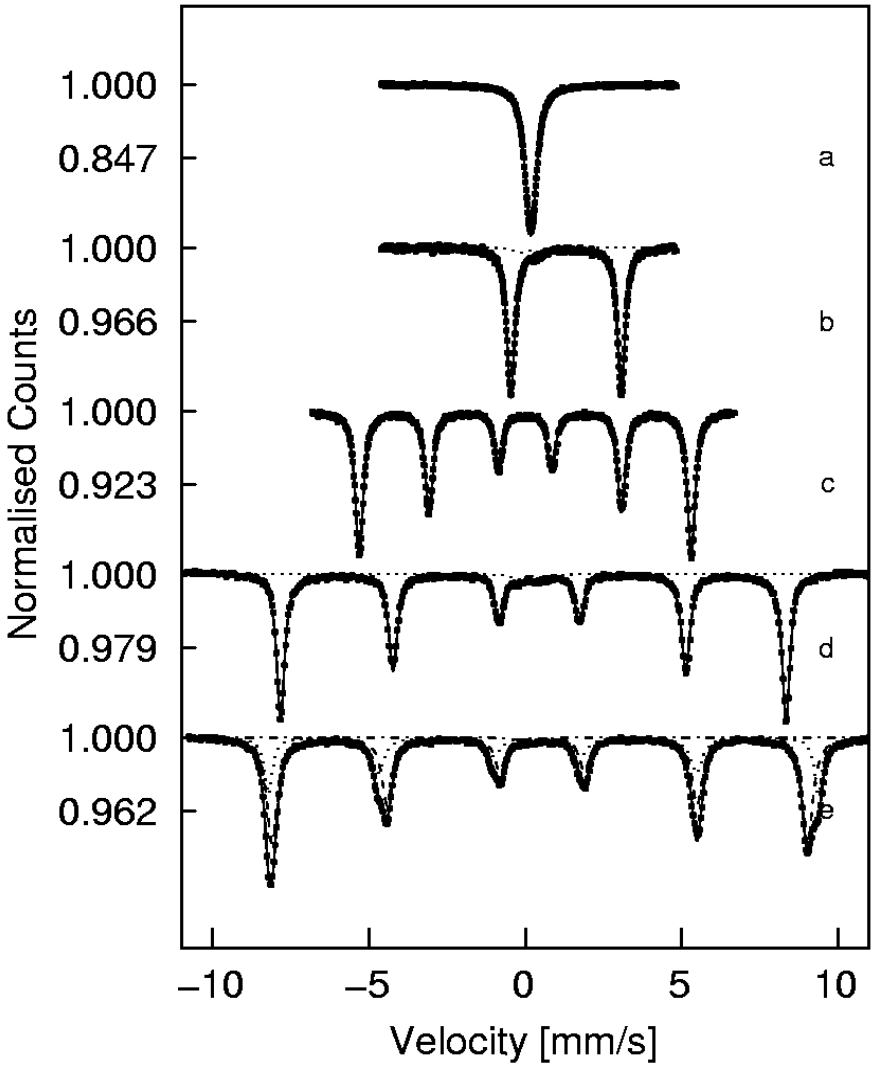

Figure 1.9. Characteristic types of ^{57}Fe Mössbauer spectra. Spectrum of (a) Pd:15at% Fe, showing an unsplit line with isomer shift, (b) almandine, showing the characteristic large quadrupole splitting of high spin Fe(II) compounds (with a very weak ferric impurity), (c) α-Fe, showing a magnetically split sextet with no quadrupole splitting, (d) hematite, showing a small quadrupole splitting accompanying magnetic splitting and (d) Western Australian "zebra rock", showing part of the hematite is above the Verwey transition and part is below, giving rise to two sextets with quadrupole splittings of the opposite signs (Cashion, unpublished data).

1.3.3 Magnetic Dipole Hyperfine Interaction

Since both the proton and the neutron have a magnetic moment, all nuclei have magnetic dipole moments, except for those with an even number of protons and neutrons, for which the ground state will have a total angular momentum, I, of zero. However, the excited states of these nuclei commonly have non-zero magnetic moments. The nuclear magnetic moment interacts with the magnetic moment of the electrons to produce the magnetic hyperfine interaction. This is essentially a microscopic or single atom magnetization measurement and is a very powerful way of obtaining information about the magnetic properties of materials. The first observation of a magnetic hyperfine splitting using ^{57}Fe Mössbauer spectroscopy was by Pound and Rebka (1959).

We do not have to consider the magnetic moments of all the electrons individually because the filled shells have zero moment and the remainder couple together according to the appropriate quantum mechanical rules to give a total magnetic moment for the atom. This moment is, of course, closely related to the overall electronic ground state of the atom. The nucleus usually sees its interaction with the electronic moment as being in an effective field.

1.3.3.1 Paramagnets

If the sample is paramagnetic, then the electronic state is switching very rapidly between its various allowed $|m_S\rangle$ levels and this usually means that the time average of the nuclear magnetization, $\langle m_J \rangle$, over the nuclear lifetime is zero, so that the nucleus does not see any magnetic field. We will deal with the exception to this, as slow paramagnetic relaxation, in Section 1.4.1.

1.3.3.2 Magnetically Ordered Materials

If the material is magnetically ordered, then $\langle m_J \rangle$ is not zero so the nucleus usually sees the electrons as a static magnetic field. The exception to this is dealt with as superparamagnetism in Section 1.4.2. The effect of a magnetic field is to completely split each of the nuclear levels into their (2I+1) components. The Hamiltonian for this interaction is

$$\mathcal{H} = -\boldsymbol{\mu}\cdot\mathbf{B}_{total} \tag{1.11}$$

where $\boldsymbol{\mu}$ is the nuclear magnetic dipole moment and $\mathbf{B}_{total}$ is the vector sum of the hyperfine field and any applied field.

The nuclear magnetic dipole moment is given by

$$\boldsymbol{\mu} = g\mu_N\mathbf{I} \tag{1.12}$$

where g is the g-value appropriate to that level, μ_N is the nuclear magneton and **I** is the angular momentum of the nuclear level. Combining equations 1.11 and 1.12, we get the expression for the energies of the (2I+1) sublevels as

$$E_i = -g\mu_N B m_i$$

where m_i takes each of the values -I, -I+1,.....,I-1, I. These splittings result in the original spectrum being split into a larger number of lines, the total number depending on the I values of the ground and excited nuclear states.

The ground state magnetic moment of ^{57}Fe is 0.09044(7) μ_N and the magnetic moment of the 14.4 keV level is -0.1549(2) μ_N (Raghavan 1989). In a magnetically split spectrum, the total splitting across the spectrum is proportional to the magnetization for a ferromagnet, or the sublattice magnetization of an antiferromagnet or ferrimagnet. For ^{57}Fe, this usually gives rise to a sextet spectrum as seen in Fig 1.9(c) which corresponds to the nuclear level diagram in Figure 1.10a. The lines are usually numbered, by convention, 1, 2,....., 6, as shown, starting with the lowest energy line.

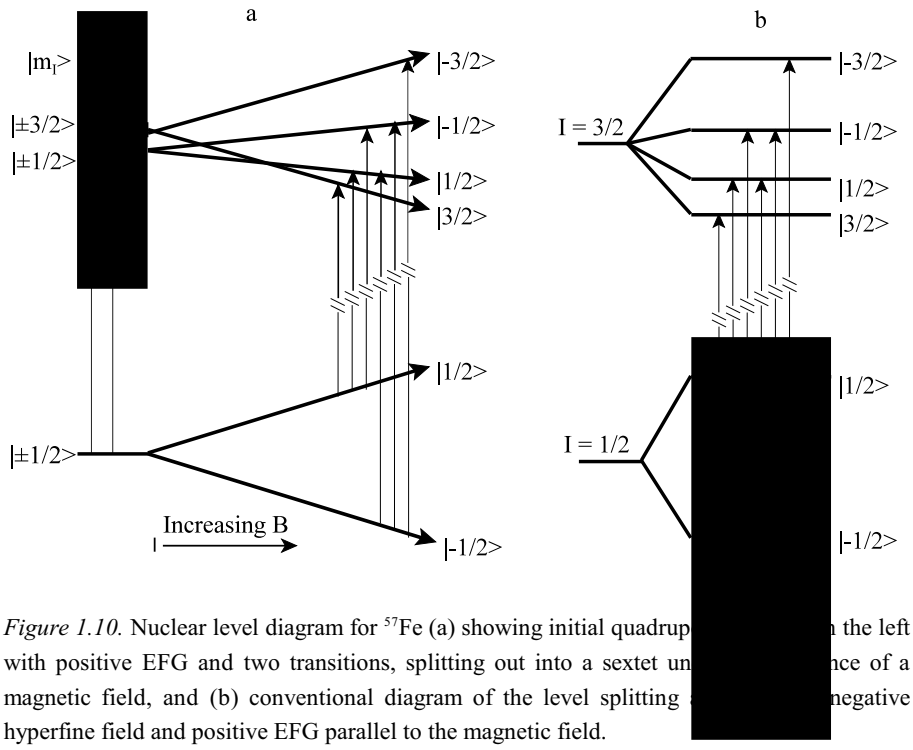

Figure 1.10. Nuclear level diagram for ^{57}Fe (a) showing initial quadrup[illegible] the left with positive EFG and two transitions, splitting out into a sextet un[illegible]nce of a magnetic field, and (b) conventional diagram of the level splitting [illegible]negative hyperfine field and positive EFG parallel to the magnetic field.

For the combined effect of a strong nuclear interaction and a much smaller quadrupole interaction, we can treat the quadrupole interaction as a perturbation to the magnetic splitting. This results in a movement of the inner 4 lines to the left and the outer two lines to the right for a positive quadrupole interaction and conversely for a negative interaction. This quadrupole shift, ε, of each line, for an axially symmetric EFG is given by

$$\varepsilon = {}^{1}/_{8}\, eQV_{zz} (3 \cos^2 \theta - 1)$$

where θ is the angle between the principal axis of the EFG and the hyperfine field or by

$$\varepsilon = {}^{1}/_{8}\, eQV_{zz} [2- (3 - \eta \cos 2\varphi) \sin^2 \theta]$$

for a lower symmetry EFG, where θ and φ are the spherical polar angles of the hyperfine field direction in the EFG principal axis system. The energy diagram for this is shown in Figure 1.10b. As an example we can see the situation for hematite in Figure 1.9d when it is above the Morin transition (see Section 5.1) and has a negative quadrupole splitting. Below the Morin transition, the quadrupole splitting changes by a factor of -2 and Figure 1.9e shows the spectrum of hematite in Western Australian "zebra rock" in which a proportion of the crystals are in each of the two states at low temperatures because of a bimodal particle size distribution.

If the quadrupole splitting is not small compared to the magnetic splitting then the total Hamiltonian, made up of the sum of the electric quadrupole and magnetic dipole Hamiltonians, cannot be solved analytically. Instead, it must be diagonalized to produce the eigenvalues (energy levels) and eigenvectors (correct linear combinations of the original $|I, m_I>$ levels) which describe the new situation. The form of the solution was first given by Kündig (1967) who showed that in the general case it is possible to obtain eight lines instead of the usual six because the mixing of the levels means that it is possible to have a $\Delta m_I = 0$ or ± 1 transition between all the four excited state levels and the two ground state levels and there are no longer any forbidden transitions.

The total splitting across the spectrum as in Figure 1.9d,e is determined by the hyperfine field - but what determines the size of the hyperfine field?

There can be four contributions to the hyperfine field and these add vectorially.

$$\mathbf{B}_{hf} = \mathbf{B}_{c} + \mathbf{B}_{sn} + \mathbf{B}_{ln} + \mathbf{B}_{ce}$$

The first contribution is the, so-called, Fermi contact term. Just as the isomer shift is due to the overlap of the charge distribution of (principally) s-electrons with the charge inside the nuclear volume, so the Fermi contact term is due to

the interaction of the magnetic moment of these electrons with the nuclear magnetic moment. Its maximum contribution is approximately -33 T. It is the dominant contribution to the hyperfine field of α-iron.

The next two contributions are from the dipole-dipole interaction of the spin and orbit parts of the electron magnetic moment with the nuclear magnetic moment. For Fe^{3+}, the orbital contribution is close to zero while the spin part gives a maximum contribution of approximately -11 T per spin making a total maximum hyperfine field of -55 T for a pure ionic Fe^{3+} ion.

The final contribution is from the conduction electrons which is fairly small and, of course, only applies to metals.

All of these contributions to the hyperfine field will normally scale closely with the magnetization (or sublattice magnetization for an antiferromagnet or ferrimagnet) so that the approximate values which we have given above are those valid at $T \approx 0$.

The reader will have noticed that the hyperfine field values quoted for iron are all negative. The implication of this will be dealt with in the next section. However, this sign was an interesting aspect of the advent of Mössbauer measurements. The numerical values of many hyperfine fields were already known from NMR measurements, but this does not give the sign. Calculation of the hyperfine field from relativistic Hartree-Fock equations was quite difficult because the relative magnitudes of the contributions from the core polarization (negative) and 3d electrons (positive) were not well known. Nevertheless, the prevailing theory at the time suggested a positive hyperfine field of the correct magnitude. When the first Mössbauer measurements on α-Fe in an applied magnetic field (Hanna *et al.* 1960) showed that the hyperfine field was negative, it caused an immediate re-evaluation of the theory (see *e.g.* Watson and Freeman 1961).

1.3.3.3 Effect of Applied Magnetic Fields

As we have already mentioned, the magnetic field measured from fitting a spectrum is the vector sum of the hyperfine field and the applied field. In all the following discussion, we shall take the applied field as defining the positive direction. The significance of the hyperfine field being negative is that the direction of the hyperfine field is opposite to that of the electron magnetization which is causing it. Thus, for example, when an external magnetic field is applied to a ferromagnet, then the field value measured from the spectrum decreases because the electron magnetization has aligned with the field and the (assumed dominant) hyperfine field is now antiparallel to the applied field. The measured field is then the difference between the two as in Figure 1.11a.

Some more complicated situations can arise. If the applied field is not along the easy axis of a single crystal ferromagnet, then the magnetization may

not be parallel to the applied field. The resultant situation is shown in Figure 1.11b where the resultant measured field is the vector sum of the two contributions and is not directed along the applied field. In a polycrystalline ferromagnet, there will be a variety of angles between the easy direction and the applied field and consequently a range of resultant magnitudes and directions for the measured field. This will result in an observable line broadening in the fitted spectrum, which can be fitted with a distribution of fields. The distribution of angles will also affect the intensities of lines 2 and 5 as described in section 1.5.3 so that it is possible, at least in principle, to obtain the distribution of fields and angles from this spectrum.

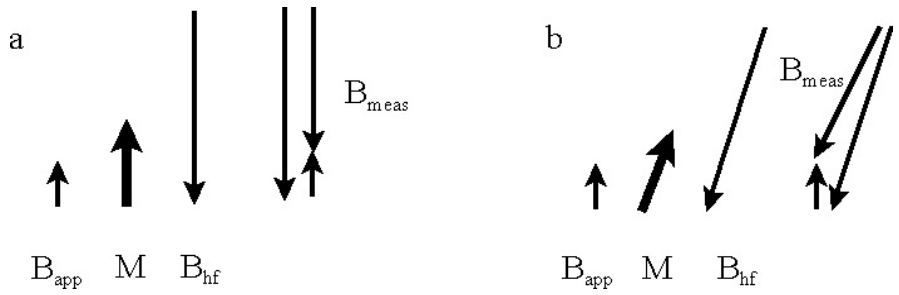

Figure 1.11. Schematic diagram showing different possible effects of an applied field on the measured hyperfine field magnitude and direction. (a) Magnetically saturated so B_{app} is parallel to the magnetization and anti-parallel to B_{hf}. (b) Not magnetically saturated so that B_{app} is not parallel to the magnetization but the latter is still anti-parallel to B_{hf}. In each case B_{meas} is the vector sum of B_{hf} and B_{app}.

Another complication can occur if the magnetization is not saturated, in other words the temperature is not sufficiently below the Curie temperature. In this case, application of a field will increase the magnetization which will, in turn, increase the hyperfine field. Thus the change in the measured field will be brought about by the increased hyperfine field (negative) and the increased applied field (positive). Knowledge of the magnetization curve would enable the contributions to be separated.

Having introduced the principles in the context of a ferromagnet, we can now treat each of the other magnetic types in turn.

In a diamagnet, the concept of anisotropy does not arise. The induced magnetization is always antiparallel to the applied field so any hyperfine field will be in the positive direction. However, the magnetic susceptibility is constant and is so small ($\sim 10^{-5}$) that the hyperfine field will be a constant factor of $\sim 10^{-5}$ times the applied field and consequently probably smaller than the uncertainty in the field calibration.

In a paramagnet, we saw in section 1.2.2 that the magnetization will approximately follow a Brillouin function dependence on B/T. This would enable an estimate of the magnetization to be made for any applied field and temperature values and then scale this by the saturation hyperfine field to give the estimated hyperfine field. The measured field should then be the difference between this field (negative) and the applied field (positive).

Ferrimagnets and antiferromagnets are more complicated because there are now (at least) two directions for the sublattice magnetizations. Thus, as seen by the electrons, this field will add to the exchange field on one sublattice and subtract from the other, unless the magnetization is exactly perpendicular to the applied field. In terms of the hyperfine field as seen by the nuclei, the changes will appear to be reversed as, for example, on the first sublattice, the positive applied field will be added to the negative hyperfine field.

In systems with multiple phases, for example several iron oxides or oxyhydroxides, one can sometimes experience difficulty in obtaining sufficient resolution to identify the phases. This can be especially true at temperatures below about 50 K, when the hyperfine fields of all the constituents are approaching their saturation values of approximately 50 T. This is where it is advisable to calculate a simulation of the predicted spectrum of each of the likely phases before doing the experiments. Choosing an optimum temperature relative to the ordering temperatures of the phases can greatly improve resolution. However, the relatively non-analytic nature of the spectra of poorly crystalline goethite at room temperature can often force one to go to lower temperatures (see Section 5.4).

In order to do these simulations, one needs to know the value of the hyperfine field at the measurement temperature. In the absence of any measurements in the desired temperature region, a good approximation can be obtained for the expected hyperfine field at a particular temperature using the general order parameter curve for the appropriate spin value (Brillouin function for S = 5/2 for Fe^{3+} or S= 2 for Fe^{2+}) and scaled to the ordering temperature on the x-axis and to the hyperfine field at T =0 on the y-axis. Then apply the preceding rules to predict the effect of the magnetic field. Examination of the spectra of all the ferric oxides and oxyhydroxides published by Pollard *et al.* (1992) and their interpretations will provide an excellent background to this exercise. Further details on the identification of poorly crystalline ferric oxides and oxyhydroxides are provided in Pankhurst and Pollard (1990, 1993) and Pankhurst (1994) and two case histories are given by Pollard (1993).

Much less use has been made of trying to choose the appropriate magnetic field value to optimize resolution. While it is possible to use Mössbauer spectra in fields to determine magnetic constants, this has only been done on a couple of occasions. Beckmann *et al.* (1968) obtained the anisotropy constant of $FePO_4$ from analysis of the spectra during field-induced spin

rotation while Mørup (1985) analysed the spin flop transition in antiferromagnetic microcrystals. In most cases, the optimum choice of field is simply the biggest available as can be seen from the spectra of Pollard *et al.* (1992). However, if one of the components undergoes a magnetic transition, then spectra just below and just above this field can be very useful. Cashion and Shannon (1998) have shown how molecular field theory can be used to predict the optimum magnetic field choice, provided that the exchange and anisotropy constants are known or can be estimated.

It should be emphasized that the Mössbauer spectrum gives two independent pieces of information about the relative directions of the (sublattice) magnetization (which is opposite to the hyperfine field), the gamma direction and the measured and applied fields. The spectrometer geometry is usually such that the gamma direction and the applied field are either parallel or perpendicular. The first piece of information is the relative areas, A_i, of lines 2 and 5 with respect to lines 1 and 6. The angle, θ, of the measured field from tl

$$\theta = \sin^{-1}\left[\frac{3A_{2,5}/A_{1,6}}{1+3A_{2,5}/A_{1,6}}\right]^{1/2},$$

The second is the vector summation to produce the value of the measured field as in Figure 1.11b. If the moments on the sublattices are collinear, the interpretation is straightforward. If there is a spread of angles, as is common in powdered ferric compounds, then information can still be obtained about the spread of angles.

There will be deviations from the simple picture presented above. Many of them are more in the vein of detailed interpretations of hyperfine interactions, than the analysis and identification of minerals and their products. Significant amongst them are how closely the magnetization follows a Brillouin function and whether the hyperfine field remains constant under the application of the applied field due to the effects of anisotropy, covalency, crystal field and how low the measurement temperature is below the ordering temperature.

1.4 Relaxation Effects

The term “relaxation effects” covers several different phenomena which all have some aspect of time dependence involved with them. Each measurement technique has a characteristic time scale and some values for common techniques are given in Table 1.4. It is important in assessing measurement data, to understand what it is which determines this characteristic time. Every solid that we study is subject to various time-dependent phenomena. Most of the phenomena are also temperature dependent. Some common examples are: atomic vibrations and their wave counterpart, phonons; electron exchange, which may or may not transfer energy; electron hopping; spin fluctuations;

energy exchange between electrons and phonons (the lattice); and so on.

Depending on the time scale of the measurement technique relative to the transition rate (inverse time) of the dynamic phenomenon, different "answers" can be obtained. In the case of Mössbauer spectroscopy there are two characteristic times to consider. The first is set by the inverse of the nuclear Larmor precession frequency, which is the frequency which the magnetic moment of the nucleus precesses in the hyperfine field appropriate at the measurement temperature. If the transition rate is slower than the Larmor frequency then the nucleus sees a static electron cloud and is able to experience the hyperfine magnetic field due to it. If the transition rate is higher than the Larmor frequency then the electron distribution alters before the nucleus can experience one complete revolution, so it does not register the hyperfine field. The second characteristic time is the mean life of the excited nuclear level, τ. Since we saw in Section 1.1.2 that this determines the resolution, then this must be longer than the Larmor precession period or we cannot resolve the structure which exists. For ^{57}Fe, the minimum experimental linewidth equals the hyperfine splitting for a field of 0.8 T. The characteristic times for some measurement techniques are compared in Table 1.4.

If a transition between two states occurs with a typical time greater than τ, then the system will be seen to be in either one state or the other when a gamma is emitted and the spectra of both cases will be superposed. However, if the transitions occur more frequently than τ then the system will be in each state for an equal fraction of τ and so the nucleus responds to the average state while it emits the gamma. The most complicated situation is when the two times are approximately the same. Then there is a statistical probability of whether an electronic transition has occurred or not and the resulting lineshapes are quite complicated, showing a gradual transition from the static spectrum to the average spectrum as the relaxation time decreases. Mössbauer spectra are most sensitive to relaxation effects when the relaxation rate is within 1-1½ orders of magnitude of the Larmor frequency.

There are three principal types of relaxation of importance in analysing and interpreting Mössbauer spectra. These are spin-spin relaxation, spin-lattice relaxation and superparamagnetism. The first two are principally of importance in dilute paramagnets and the last in fine particle, magnetically ordered materials.

The most commonly used model for describing relaxation lineshapes is due to Blume and Tjon (1968). This assumes that the magnetic hyperfine interaction is between the nuclear magnetic moment and a time-dependent magnetic field which changes stochastically.

There have been many excellent reviews on relaxation effects in Mössbauer spectroscopy. Some of the more extensive are by Wickman (1966), Wickman and Wertheim (1966, 1968), Blume (1968), Wegener (1975),

Dattagupta (1983), Bhargava (1983), Kolk (1984), Hoy (1984), Mørup (1981, 1982, 1990) and Jones (1989) and the reader is referred to these for more details.

Let us now look at the effect of each of these relaxation mechanisms on the Mössbauer spectrum.

Table 1.4. Characteristic times and frequencies for different measurement techniques.

Technique	Characteristic time	Characteristic frequency	Determining factor
Magnetization (*e.g.* dc squid)	0.1 - 1 s	1 - 10 Hz	Response of electronics
AC susceptibility	0.01s	100 Hz	AC frequency
NMR	$\gtrsim$1 μs 1-100 ns	$\lesssim$MHz 10-700 MHz	Nuclear T_1, T_2 Oscillator frequency = nuclear precession frequency

Mössbauer effect	30 ns (in 50 T hyperfine field for ^{57}Fe) 100 ns (^{57}Fe)	34 MHz	Nuclear precession frequency Mean life of nuclear
EPR	$\gtrsim$1 ns 2-300 ps	$\lesssim$GHz 3-200 GHz	Electronic T_1, T_2 Klystron frequency = electron precession frequency
Neutron scattering	10 fs	~10^{14} Hz	Interaction time with nucleus or electrons
X-ray scattering	10 fs	~10^{14} Hz	Interaction time with electrons
IR spectroscopy	10 fs	~10^{14} Hz	Phonon frequencies
Optical spectroscopy	0.1 fs	~10^{16} Hz	Electron excitation time
XPS	0.1 fs	~10^{16} Hz	Electron excitation time for emission

1.4.1 Slow Paramagnetic Relaxation

Spin-spin relaxation occurs between neighbouring magnetic atoms and involves an exchange of energy between them. If they were both systems with electronic spin ½,, then we could imagine a transition from the configuration with the two spins being “up-down” to “down-up”. We could represent this as

$$s_{1\uparrow}\, s_{2\downarrow} \rightarrow s_{1\downarrow}\, s_{2\uparrow}.$$

In the case of high spin Fe^{3+}, which has a ladder of six equally spaced Zeeman levels, there is a large range of possible up and down transitions which satisfy the requirements. The interactions always involve only the z-components of the spins and there is no net loss of energy to the spin system. The spin-spin relaxation time, usually denoted by t_1, does not depend on temperature, except through the population of the electronic levels, but it does depend on the mean distance between the spins, *i.e.* the concentration of paramagnetic ions.

Dynamic crystal field effects can generate two different modifications to the Mössbauer spectra of high spin iron species. The most common is the creation of time-dependent effects through spin-lattice relaxation, which

enables transitions between the electronic states of the ion. In spin-lattice interactions, energy is transferred from the spin system to the lattice (phonons) via the spin-orbit and orbit-lattice interactions. Thus it is much more efficient in Fe^{2+} and low spin Fe(III) than in the S-state Fe^{3+}. Since the population of phonon states is very temperature dependent, the spin-lattice interaction time, usually called t_2, is also temperature dependent.

The second crystal field effect is through vibronic coupling which gives a quasi-static admixture of the electronic levels of the ion and is approximately time-independent. However, it is temperature dependent through the amplitude of the lattice vibrations. The effects of vibronic coupling are complicated and the best known manifestation is the Jahn-Teller effect, although this is not so common for Fe^{2+} as it is for some other transition metal ions. In Mössbauer spectra, vibronic coupling can give rise, for example, to temperature dependent changes in the quadrupole splitting and small asymmetries in the linewidth of quadrupole split doublets of high spin Fe^{2+} materials, which can often be erroneously explained by relaxation effects, unless analysis of results from several different techniques are carried out consistently. An excellent survey of the effects of static and dynamic crystal field effects and their observation in Fe^{2+} Mössbauer spectra has been given by Price and Varret (1983) and a detailed evaluation of its effects, applied to ferrous fluosilicate, by Price (1987).

In all the preceding discussion of the magnetic hyperfine interaction, we have assumed that the nucleus will view this as an effective field. In reality, the Hamiltonian for the magnetic hyperfine interaction should be written as

$$\mathcal{H} = \underline{\mathbf{S}} \cdot \underline{\underline{A}} \cdot \underline{I}$$

rather than the simple form in Equation 1.11, and this reduces to the effective field approximation if there is either a strongly anisotropic Kramers doublet ($g_z \gg g_x, g_y$) or an external magnetic field which gives an electronic splitting much larger than the hyperfine interaction. In a paramagnet, neither the magnitude nor the direction of the effective field is fixed - they fluctuate due to relaxation.

Let us first consider an Fe^{3+} ion in a simple crystal field given by the Hamiltonian

$$\mathcal{H} = D [S_z^2 - 1/3\ S(S+1)]$$

This will split the S = 5/2 level into three doublets which can be described by their S_z values as $|\pm 5/2\rangle$, $|\pm 3/2\rangle$ and $|\pm 1/2\rangle$. They will be arranged in order, with the $|\pm 5/2\rangle$ states at the bottom if D is negative and reversed if D is positive, where typical values for $|D|/k_B$, in temperature units, are 0.01-1 K.

If the electrons remain in one of these levels for a time longer than τ, then the nucleus will "see" a hyperfine field of (-11 T) times the spin value. There is thus the possibility of six different field values but three only differ in sign, which is not immediately detectable. However in the presence of an

applied magnetic field, these will all become different because of the vector addition discussed in section 1.3.4.3.

Relaxation processes can only change the S_z values by ±1. Thus relaxation is forbidden between the degenerate |+5/2> and |-5/2> levels, and similarly between |+3/2> and |-3/2>. However, it is allowed between |+1/2> and |-1/2> so that these are only rarely observed as hyperfine split levels. Relaxation between different doublet states requires the transfer of energy and hence is temperature dependent. Increase in temperature causes the spectral structure to gradually collapse down to the normal paramagnetic state, which is usually a doublet. One other situation can occur when the $S_z = |\pm½>$ state is the lowest. The relaxation is fast at low temperature, when only this doublet is populated, but becomes slower as the other two doublets become populated resulting in an asymmetrical broadening of one line of the doublet (Blume 1967).

The simple axial crystal field described above will frequently have a rhombic distortion. Although there are still three doublets, these are no longer describable by single $|S_z>$ states and the possibilities become much more complicated. We refer readers to the excellent reviews by Wickman (1966), Wickman and Wertheim (1966, 1968), Mørup (1981, 1982, 1990).

Examples of slow paramagnetic relaxation have been found in iron doped synthetic corundum (Johnson *et al.* 1965, Wickman and Wertheim 1966), natural kaolinite (Fysh *et al.* 1983a), brown coal (Bocquet *et al.* 1998) and montmorillonite (Murad *et al.* 2002), but is it generally uncommon in natural minerals because of the fairly strict requirement on a uniformly distributed and quite low iron concentration.

1.4.2 Superparamagnetism

Both spin-spin and spin-lattice relaxation operate via transitions involving single spins. A cooperative change in the magnetization of a group of spins occurs, for example, when we magnetize a material and all the moments in a magnetic domain or particle rotate together. On a smaller scale, this is what happens when we write to a computer disk and a small number of magnetic particles (a few hundred) all reverse their magnetization to constitute each bit. The energy required to reverse the magnetization of a particle depends directly on its volume and can be thought of as a barrier of height K_eV, where K_e is the effective magnetic anisotropy constant and V is the volume. For materials with uniaxial anisotropy, K_e is the uniaxial anisotropy constant, while for cubic anisotropy described by an anisotropy constant K, K_e is equal to K/4 for K>0 (<100> easy axis) and K/12 for K<0 (<111> easy axis). As the particles become smaller, the energy barrier becomes comparable with the thermal energy, k_BT, and the frequency for the spontaneous reversal of the

magnetization is given by (Néel 1949):

$$f = f_0 \exp(-KV/k_BT)$$

where f_0 is a poorly characterized frequency of order 10^8 - 10^{12} Hz which is dependent on the temperature and the volume, magnetization and K_e of the material (Aharoni 1969, Jones and Srivastava 1989).

The corresponding critical size of approximately 10 nm is quite common in precipitating systems, including both natural and mineral processing samples. The size of magnetic particles in computer disks has also practically reached this limit - which is a problem since we don't want our disks rewriting themselves on a hot day!

As described in section 1.4, if the magnetization reversal is fast enough, then the nucleus sees a time averaged field of zero over the Larmor precession period instead of the magnetic hyperfine structure of a magnetically ordered material. In the intermediate region, the spectrum is complex. Also, most materials will contain a range of particle sizes and these will pass through the critical frequency range at different temperatures. This can provide a method of obtaining a crude histogram of particle sizes in the region 3-20 nm. However, the appropriate description of the physical process changes from that of collective excitations (Mørup 1983), valid up until the smallest diameter particles start to reverse their magnetization, to that of spin flips (Blume and Tjon 1968) valid when all the particles, including the largest, are flipping. In the interesting intermediate region, a many state relaxation model must be used (Jones and Srivastava 1986, 1989, van Lierop and Ryan 2000, 2001a).

A characteristic temperature, called the (superparamagnetic) blocking temperature, is often used to describe superparamagnetic systems, particularly as an effective measure of their mean particle size. It is usually taken as the temperature at which there are equal areas in the magnetically split and quadrupole doublet parts of the spectrum, or alternatively, equal areas in the magnetic sextet and magnetically relaxing parts of the spectrum. However, the many state relaxation model used by van Lierop and Ryan (2000, 2001a) uses the temperature at which superparamagnetic relaxation begins, which gives a value consistent with that derived from other techniques such as the frequency dependent magnetic susceptibility. They obtained values of 100 MHz and 220 MHz for the frequency f_0 for two magnetite-based ferrofluids.

There are other relaxation processes, which are often loosely, and incorrectly, classified under the umbrella of superparamagnetism. An example is poorly crystalline or aluminous goethite which produces very characteristic asymmetrically broadened spectra (see *e.g.* Mørup 1981) which are inconsistent with the lineshape of superparamagnetic spectra. One effect of nanoscale dimensions in antiferromagnets is that there is no longer the

statistical expectation that the number of magnetic moments pointing in the two opposite directions will be exactly equal. This means that the particles have a small net magnetic moment and these "supermoments" on adjacent particles are correlated due to interparticle magnetic interactions. It is possible that the dwell times in the two states of reversed magnetization are not always identical (Rancourt and Daniels 1984, Rancourt 1988) and while this will produce changes to the Mössbauer spectra, it is still unclear to what extent this occurs in practice.

Mørup *et al.* (1983) analysed the spectra of poorly crystalline goethite by including the exchange coupling between particles under the name "superferromagnetism". Using a distribution of hyperfine fields (see Section 3.6), excellent fits were obtained to the spectra.

An alternative approach is to consider that crystals of this type are not strictly single particles. Rather, the replacement of iron atoms by either diamagnetic atoms such as aluminium or by vacancies causes breaks in the magnetic interaction paths which couple the iron atoms (Murad 1979). This creates individual "clusters" of antiferromagnetically aligned atoms whose magnetization vector can reorient under thermal excitation.

Bocquet *et al.* (1992) considered that the breaks in the exchange paths allowed the material to be described as clusters whose effective size is a function of temperature, becoming larger with decreasing temperature. These clusters then have a variable height energy barrier to overcome in order to reverse their magnetization. Excellent fits were obtained, including to the same data as used by Mørup *et al.* (1983).

1.4.3 EFG Relaxation

Fluctuations in the EFG can occur due to several causes, such as dynamic Jahn-Teller distortion, movement of a nearby atom, ion, or vacancy, or an electronic relaxation process in a neighbouring ion. Note that these latter processes do not involve the Mössbauer atom specifically - these cases are dealt with under diffusion (Section 1.6) and electron hopping (Section 1.4.4). The original theory was due to Tjon and Blume (1968) and they considered the cases where the EFG changed direction as a random function of time either by reversing its direction along the z-axis or by switching between the x, y or z axes as would occur in the jump of a nearest neighbour vacancy in a cubic crystal. The slow relaxation limit is, naturally, a quadrupole split line and this gradually collapses down to a single line as the relaxation frequency increases.

1.4.4 Charge Transfer

Dynamic charge transfer or electron hopping between adjacent cations is quite

common in minerals and can be thermally or optically activated. For thermally activated processes, the hopping can simply reverse the valency of two atoms of the same type, *e.g.*

$$Fe^{2+} + Fe^{3+} \rightleftharpoons Fe^{3+} + Fe^{2+}$$

or between two different kinds of atoms, *e.g.*

$$Fe^{2+} + Ti^{4+} \rightleftharpoons Fe^{3+} + Ti^{3+}$$
$$Fe^{2+} + Mn^{3+} \rightleftharpoons Fe^{3+} + Mn^{2+}$$

If the electron dwell time is shorter than the nuclear lifetime, then the isomer shift will be an average of those for the two valency states. This may be an anomalous value which cannot be obtained or is very rare in static spectra, such as the isomer shift of 0.67 mm/s for the octahedral site in magnetite. However, if the electron dwell time is longer than the nuclear lifetime, then the situation appears static and a superposition of the subspectra of each of the two valency states is seen. In cases where the times are comparable then a series of spectra taken at different temperatures will show a transition between the two limiting cases.

Thermally activated hopping between two iron ions requires the ions to be in similar or equivalent, adjacent, edge-sharing polyhedra, which must form extended structural units (Amthauer and Rossman 1984). Examples are deerite, $Fe_6^{2+}Fe_6^{3+}O_3Si_6O_{17}(OH)_5$, (Amthauer *et al.* 1980), vonsenite, $Fe_2^{2+}Fe^{3+}BO_5$, (Swinnea and Steinfink 1983) and ilvaite, $CaFe_2^{2+}Fe^{3+}Si_2O_8(OH)$, (Litterst and Amthauer 1984).

For optically activated processes, the sixth d-electron on an Fe^{2+} can be excited up to the energy which corresponds to it being distantly trapped on a neighbouring, currently, Fe^{3+}. There will then be an ensuing lattice re-arrangement to accommodate the new ionic sizes. The deep blue colour in vivianite, $Fe_3^{2+}(PO_4)_2.8H_2O$, is due to charge transfer between an Fe^{2+} and an Fe^{3+} in adjacent edge-sharing octahedra (Vochten *et al.* 1979). Fe^{3+} also exists on the single octahedron site but does not participate in the charge transfer.

Note that these processes are different from the thermally and optically activated spin crossover (high spin to low spin) transitions (see, *e.g.*, Gütlich *et al.* 1994) exhibited by a number of iron organic materials. A more complicated example of a mixed charge distribution is provided by $FeTi(SO_4)_3$ which was expected to be $Fe^{2+}Ti^{4+}(SO_4)_3$. However, the Mössbauer spectra showed that it was really static $(Fe^{2+}_{1-y}\ Fe^{3}_{y+})(Ti^{3}_{y+}Ti^{4+}_{1-y})(SO_4)_3$ (Gibb *et al.* 1968).

1.5 Line Intensities

There are two main aspects of line intensities. The first is the absolute magnitude of the absorption compared to the baseline while the second is the relative intensity of different lines which are part of the same hyperfine split

spectrum. In understanding the first aspect, in Section 1.5.1 we will deal with the f-value and the thickness of the absorber, but leave the techniques for determining the optimum absorber thickness until Section 2.6.3. The relative intensities depend on the Clebsch-Gordan coefficients (Section 1.5.2), the angular dependence of the gamma radiation (Section 1.5.3), the effects of texture in the sample (Section 1.5.4) and the angular dependence of the f-value, which is also known as the Goldanskii-Karyagin effect (Section 1.5.5).

1.5.1 Recoilless Fraction and Thickness Effects

We have already dealt with the principles of the f-value in section 1.1.1. Clearly, the larger the f-value of both the source and the absorber, then the higher will be the proportion of gamma rays which will be absorbed recoillessly. The expression for the intensity of transmitted radiation through a resonant absorber was first given by Margulies and Ehrman (1961). The source emits gammas which have an f-value of f_s. Both the resonant and non-resonant gammas are subject to electronic absorption on passing through the absorber, with the normal exponential dependence on thickness. In addition, the resonant gammas are also subject to nuclear resonant absorption whenever the ıe exp ın by

$$I(v) = (1 - f_s) + \frac{2f_s}{p\Gamma}\int_{-\infty}^{\infty} \frac{\Gamma_s^2/4}{(E - E_{0s})^2 + \Gamma_s^2/4} \times \exp\left[\frac{-T_a \Gamma_a^2/4}{(E - E_{0a} + v)^2 + \Gamma_a^2/4}\right] dE \qquad (1.13)$$

where E_0 is the resonant energy, v is the velocity in energy units and the subscripts "s" and "a" refer to the source and absorber respectively. This expression is usually referred to as the **transmission integral**. The quantity T_a is the dimensionless effective thickness of the absorber and is given by

$$T_a = f_a\, n_a\, a_a\, \sigma_0\, t_a$$

where n is the number of atoms of the Mössbauer element per unit volume with isotopic abundance fraction, a, σ_0 is the resonant absorption cross-section at resonance and t_a is the linear thickness. For ^{57}Fe, $\sigma_0 = 257 \times 10^{-20}$ cm^2.

If the absorber is very thin, then the exponent can be expanded and the integral simply becomes a Lorentzian of width ($\Gamma_s + \Gamma_a$) and the depth of the dip depends on the product of f_s, f_a and t_a. However, if the absorber is made thicker so that this approximation is no longer valid, the line becomes broader and non-Lorentzian. Further details on this are given in Section 2.6.3 and Chapter 3.

A schematic diagram of how the resonant and non-resonant contributions make up the Mössbauer spectrum is given in Figure 1.12.

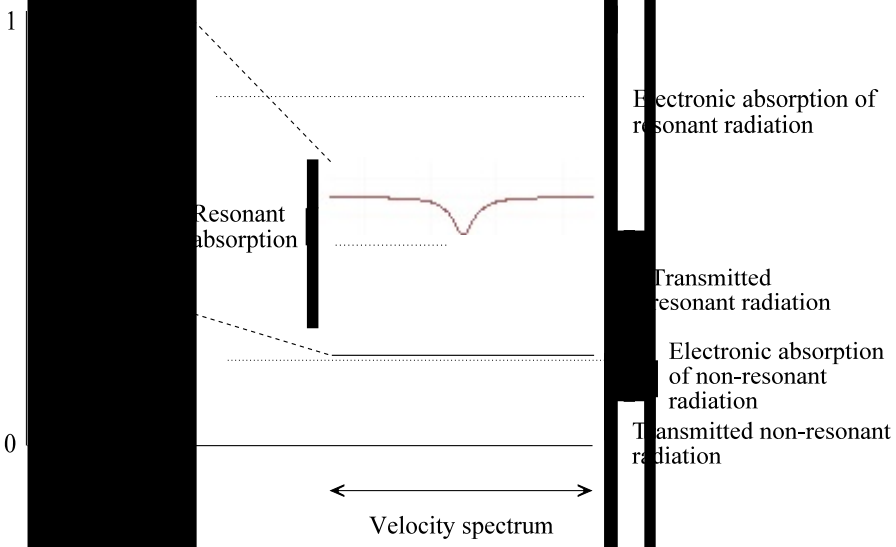

Fig atic diagram showing how the initial radiation intensity, taken to have a rec ~ 0.7, is modified on passing through the absorber by resonant absorption an ption and scattering. The absorber thickness has been chosen to allow 70% tra what larger than the usual optimum. For vari scattering and Compton sca hich result in the detection of additional photons within the 14.4 keV wi gnored.

ority of Mössbauer experiments, it is not necessary to know the nsity of the absorption with any accuracy – it is principally the va rfine parameters which are important. However, the intensity is ant for quantitative analysis. In this section we will merely me cipal effects of thickness on the absorption lines and leave it un .4 and 3.5 to see how these effects should be dealt with qu

esonant part of the gamma ray beam passes through the ab nsity will be attenuated. However, its shape is also changed be sorber is at a resonant velocity, we can think of the situation as being absorbed from the centre of the beam than from the wi vely thin absorbers, the flux lineshape will still be able to be fit ntzian, but the line gets shorter and fatter resulting in an inc dth.

dening has other effects on the spectral analysis, such as mo ed line positions from their true values when there are ov s and an inappropriate algorithm has been used to fit the sp g the incident flux through a single crystal absorber also has

the effect of polarizing the beam, which then modifies the relative line intensities in the spectrum. A lot of effort has been put into analysing these effects and devising the most efficient method of computing them - a situation which has changed considerably over the past thirty years with the dramatic improvements in computing power. More complete details are given in Sections 3.4 - 3.6.

1.5.2 Relative Intensities of Hyperfine Split Lines

In the Mössbauer spectrum of α-iron (Figure 1.9c), it can be seen that the intensities follow a pattern. These relative intensities are given by the squares of the angular momentum coupling coefficients known as the Clebsch-Gordan coefficients or 3j symbols. The values of these depend on the angular momenta of the two nuclear states and of the gamma ray. For the |3/2> to |1/2> transitions which we have been considering, the gamma ray takes off one unit of angular momentum. If we denote the transitions by the z-components of the angular momentum of the excited and ground states, then for the six allowed transitions in the α-iron spectrum, the relative intensities have the values

$$\begin{array}{lcclcl} I(|3/2> \rightarrow |1/2>) & = & 3 & = & I(|-3/2> \rightarrow |-1/2>) \\ I(|1/2> \rightarrow |1/2>) & = & 2 & = & I(|-1/2> \rightarrow |-1/2>) \\ I(|1/2> \rightarrow |-1/2>) & = & 1 & = & I(|-1/2> \rightarrow |1/2>) \end{array}$$

Simple quadrupole split spectra (Figure 1.9b) are made up of the first two transitions in one line and the remaining four transitions in the other, and these can be seen to have equal intensity.

These values are only valid as long as the hyperfine field and any EFG are parallel. If they are not, then these coefficients (as amplitudes rather than intensities) must be used with a diagonalization of the full Hamiltonian in order to calculate the line intensities. Under these circumstances, it is possible for the original six lines to increase to eight because the new nuclear wave functions are linear combinations the original pure $|m_I>$ states. The first computer program to fit spectra using this technique was by Gabriel and Ruby (1965) and the first systematized presentation of the results of these calculations was by Kündig (1967) (see also Hofmann *et al.* 1977, and Le Caër *et al.* 1978). An analytical solution was developed by Arif *et al.* (1975) when the quadrupole splitting is small compared to the magnetic splitting. An improved and faster analytical solution of the secular equation was developed by Häggström (1974) as the solution to a quartic equation. An alternative solution method using superoperators, which yields closed form expressions for the Mössbauer lineshape without diagonalizing the secular equation, was published by Blaes *et al.* (1985)

An important, and still underappreciated, limitation for the case of arbitrary angles between the total magnetic field, the EFG tensor and the gamma ray direction is that there is not sufficient information in the Mössbauer spectrum to evaluate all the parameters uniquely. Only the magnetic field, the isomer shift and quadrupole splitting ($\frac{1}{2}eQV_{zz}[1 + \eta^2/3]^{1/2}$) are unambiguously determined, with the angles having ranges of allowed values as function of η. These must be systematically searched for, as was first recognized by Karyagin (1966) and it is possible to find a completely valid, but non-unique fit to a spectrum. (Note the error in two equations in the English translation of Karyagin (1966) as pointed out in van Dongen Torman *et al.* 1975).

1.5.3 Angular Dependence and Polarization of Lines

The emission of a photon has an angular probability distribution with respect to the direction of the dominant source of anisotropy affecting the emitting atom or nucleus. The form of the angular dependence is determined by the angular momentum taken off by the photon. The following rules apply only to the $|^3/_2>$ to $|^1/_2>$ dipole transitions such as ^{57}Fe. Other dipole transitions will have the same angular form for the different Δm values, but there will be a different total number of transitions. However, not all Mössbauer transitions are dipole transitions, for example the $|2>$ to $|0>$ transitions common in the rare earth nuclides, for which the following formulae will not be valid.

Table 1.5 lists the angular functions, $g(\theta)$, for all the different combinations of excited and ground state magnetic quantum numbers. The change in the magnetic quantum number for absorption is listed as Δm, while the squares of the Clebsch-Gordan coefficients, normalized to unity are given in the next column. The two transitions with $\Delta m_I = 2$ are forbidden, since a

Table 1.5. Angular functions, polarization and relative intensities for the spectral lines in a |3/2> to |1/2> transition.

Magnetic sextet (with $V_{zz} = 0$ or V_{zz} parallel to B_{total} and $\eta=0$)

$I = {}^3/_2$	$I = {}^1/_2$	Δm	$(CG)^2$	$g(\theta)$	Relative line intensities (and polarization)		
I_z	I_z	(abs)			$\gamma \parallel B_{total}$	$\gamma \perp B_{total}$	Random
${}^3/_2$	${}^1/_2$	+1	${}^1/_4$	${}^3/_4(1+\cos^2\theta)$	3 (RH)	3 ($\parallel$)	3
${}^1/_2$	${}^1/_2$	0	${}^1/_6$	${}^3/_2\sin^2\theta$	0	4 ($\perp$)	2
$-{}^1/_2$	${}^1/_2$	-1	${}^1/_{12}$	${}^3/_4(1+\cos^2\theta)$	1 (LH)	1 ($\parallel$)	1
$-{}^3/_2$	${}^1/_2$	(-2)	0	-	-	-	-
${}^3/_2$	$-{}^1/_2$	(+2)	0	-	-	-	-
${}^1/_2$	$-{}^1/_2$	+1	${}^1/_{12}$	${}^3/_4(1+\cos^2\theta)$	1 (RH)	1 ($\parallel$)	1
$-{}^1/_2$	$-{}^1/_2$	0	${}^1/_6$	${}^3/_2\sin^2\theta$	0	4 ($\perp$)	0

$^{-3}/_{2}$	$^{-1}/_{2}$	-1	$^{1}/_{4}$	$^{3}/_{4}(1+\cos^2\theta)$	3 (LH)	3 (∥)	3

Quadrupole doublet (with $\eta=0$)

					$\gamma \| V_{zz}$	$\gamma \perp V_{zz}$	Random
$\pm^{3}/_{2}$	$\pm^{1}/_{2}$	± 1	$^{1}/_{2}$	$^{3}/_{4}(1+\cos^2\theta)$	3 (π)	3 (π)	3
$\pm^{1}/_{2}$	$\pm^{1}/_{2}$	$0, \mp 1$	$^{1}/_{2}$	$^{5}/_{4}-^{3}/_{4}\cos^2\theta$ $^{1}/_{2}+^{3}/_{4}\sin^2\theta$	1 (σ)	5 (σ)	3

Quadrupole doublet (with $\eta \neq 0$)

$\pm^{3}/_{2}$	$\pm^{1}/_{2}$	± 1	$(1+\eta^2/3)^{1/2} + (3\cos^2\theta - 1 + \eta \sin^2\theta \cos 2\varphi)/4$	3
$\pm^{1}/_{2}$	$\pm^{1}/_{2}$	$0, \mp 1$	$(1+\eta^2/3)^{1/2} - (3\cos^2\theta - 1 + \eta \sin^2\theta \cos 2\varphi)/4$	3

dipole transition can only take off one unit of angular momentum. The product of the terms in this column with the g(θ) term gives the angular dependence of the transition.

The final three columns give the relative line intensities for three common cases. For the magnetic sextets, we first consider the gamma direction to be parallel or perpendicular to the total magnetic field on the nucleus in a fully magnetized sample or, in the last column, assume that the magnetization is completely random. In the case of the quadrupole split spectra, the relative intensity of the two lines are given for a single crystal aligned parallel or perpendicular to V_{zz} (with $\eta = 0$) or alternatively for a powder sample. The two sets of average values are obtained from the g(θ) values by the integrating each over a sphere as

$$< f(\theta) > \quad = \quad \frac{1}{4\pi}\int_0^{2\pi}\int_0^{\pi} g(\theta)\, \sin\theta \; d\theta \, d\phi$$

and the values scaled to integers.

The change in intensity of lines 2 and 5 of the magnetic spectrum can be used to obtain information about the average direction of the total magnetic field, or by vector analysis, the average direction of the magnetization.

Similarly, the different intensities of the quadrupole split lines in a single crystal can be used to determine the sign of the EFG, which cannot be done from a powder specimen.

For single crystals, the lines are polarized for both magnetic and quadrupole splitting and the type of polarization is also given in Table 1.5. This polarization of the absorption means that an initially unpolarized beam will become progressively polarized as it passes through the absorber (Nussbaum and Housley 1965, Housley *et al.* 1969). Note that the total area of the spectrum changes under these different scenarios; it is not just a redistribution of intensity between the lines. Failure to include the effects of polarization in the analysis has resulted in mistakes in the literature as pointed out by Housley *et al.* (1968). Regrettably, this mistake is almost as likely to occur now as it was over thirty years ago.

The fractional polarization, for the quadrupole split case with $\eta = 0$, is given by (Housley *et al.* 1968)

$$a_\pi(\theta) = \sin^2\theta / (1+\cos^2\theta)$$

and

$$a_\sigma(\theta) = 3\sin^2\theta / (5 - 3\cos^2\theta).$$

Note that the total cross section, that is, the product of g(θ) a(θ), is the same for the two polarizations.

1.5.4 Texture Effects on Line Intensities

In the preceding section we have seen that the line intensities depend on the

angle of the principal hyperfine interaction to the direction of the gamma ray. The situation is analytical if there is a single angle or if all angles are equally probable. But what happens if one has a sample whose morphology is fine needles or thin plates? If these are placed into an absorber holder, then we will not have a random powder because of the preference of these shapes to lie flat in the holder. Even crushing them up quite finely and mixing with a filler may not remove all traces of preferential orientation, particularly if the sample is compressed. A similar effect can occur in metal foils where mechanical treatment such as rolling will give a preferential orientation of some crystallographic directions in the plane of the foil.

Texture and the Goldanskii-Karyagin effect, which is treated in the next section, both produce a very similar effect on the line intensities, as was first detailed by Pfannes and Gonser (1973), triggered partly by the conflicting interpretations on the spectra of siderite, $FeCO_3$.

There are many different possible distribution functions which could describe the non-random orientation of crystallites in an absorber. Let us start by assuming a crystal with a unique axis "c". This axis has a general distribution function $D(\theta)\, d\Omega$, such as might be measured by XRD, where $D(\theta,\varphi)$ is the relative volume of crystallites oriented with their c-axes in the solid angle $d\Omega$ centred at the polar angle, θ, φ with respect to the gamma ray direction. For a transmission experiment, all crystallites with their axes in the cone between θ and $\theta + d\theta$ will give the same spectrum. Thus the φ dependence can be eliminated and the area of the annular rings increases proportional to $\sin \theta$, so this can be used to weight the distribution.

The distribution can then be multiplied by the various $g(\theta)$ functions and integrated to obtain the expected relative line intensities. However, we are more usually interested in coming from an experimental set of line intensities which we wish to interpret in terms of a $D(\theta)$. There is no unique solution to this problem. However, if we assume a particular functional form for $D(\theta)$, then we can usually evaluate the assumed parameter in the distribution. The relation of these parameters to reality is completely dependent on the validity of the choice of the original function.

However, further information can be obtained by taking many spectra with the absorber tilted at various angles to the gamma beam and solving the equations as a histogram (Gonser and Pfannes 1974). If the assumption of conical symmetry is not valid, then this can also be tested for by rotating the specimen at a set angle. As a means of obtaining information on preferred orientation, it is not competitive with XRD, but the consequences of ignoring the deleterious effects of texture on the interpretation of Mössbauer spectra should not be underestimated.

If a spectrum is taken at the so-called "magic angle" of 54.7° to V_{zz} or to B_{total}, then one obtains the same intensities as one would get in a powder

(see, for example Figures 1 and 3 in Pfannes and Gonser 1973). This led first to the technique of taking a spectrum with the sample tilted at 54.7° to the gamma beam, which eliminates all texture with conical symmetry (Ericsson and Wäppling 1976). Further, if one takes four spectra, rotating the sample by 90° in the plane of the tilted absorber holder between each one, and then sums the spectra, the resulting spectrum will be free of all texture effects (Grenèche and Varret 1982).

1.5.5 Goldanskii-Karyagin Effect

In our introduction to the recoilless fraction (section 1.1.1), we assumed that it had the same value in all directions. However, if we look at its dependence on the r.m.s. amplitude

$$f = \exp [-k^2 \langle x^2 \rangle] \qquad (1.6)$$

and we take a sample for which the r.m.s. amplitude is different in different directions, for example, compounds with linear or planar bonding, then we can expect that the f-value will also be directionally dependent. Is the difference large enough to be significant?

It is usual to assume that the vibrational amplitude is axially symmetric with values $\langle x_{\parallel}^2 \rangle$ and $\langle x_{\perp}^2 \rangle$ parallel and perpendicular to the axis of symmetry, respectively. Then we can write the f-value as (Karyagin 1963, Goldanskii and Makarov 1968)

$$f'(\theta) = \exp [-k^2 \langle x_{\perp}^2 \rangle] \exp [-k^2 (\langle x_{\parallel}^2 \rangle - \langle x_{\perp}^2 \rangle) \cos^2 \theta]$$

where only the second term depends on θ.

The relative intensities of the two lines in a quadrupole split doublet can then be determined by the integration of this function multiplied by the angular functions from

$$\frac{I(^3/_2)}{I(^1/_2)} = \frac{\int_0^{\pi} f'(\theta)\,(1+\cos^2\theta)\,\sin\theta\,d\theta}{\int_0^{\pi} f'(\theta)\,(^5/_3 - \cos^2\theta)\,\sin\theta\,d\theta}$$

A plot of this ratio, as a function of $k^2 (\langle x_{\parallel}^2 \rangle - \langle x_{\perp}^2 \rangle)$ is shown in Figure 1.13 (from Goldanskii and Makarov 1968). In practice, one rarely finds cases which are outside the enlarged part of the diagram in the inset.

Definite cases of the observation of the Goldanskii-Karyagin effect for ^{57}Fe materials are very rare, although it has been invoked much more frequently to explain asymmetric doublets. In spite of many searches, the first observation in a silicate was not until 1992, in almandine (Geiger *et al.* 1992). Other definite observations were in $FePS_3$ (Chandra and Ericsson 1979) and in $Fe_3(CO)_{12}$ (Grandjean and Long 1996). However, for ^{197}Au, and for a lesser extent for ^{119}Sn, asymmetric doublets due to the Goldanskii-Karyagin effect are relatively common, helped by their linear and planar bonding and higher

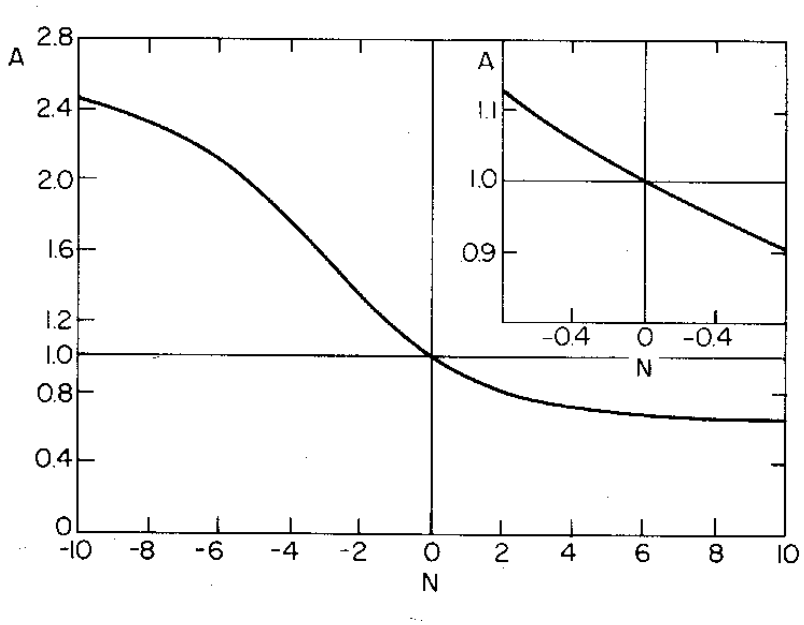

energy transitions.

Figure 1.13. Dependence of A, the relative intensities of the ($\Delta m = \pm 1$ line)/($\Delta m = 0$ line), on the difference in the mean square amplitude, $(\langle x_{\parallel}^2 \rangle - \langle x_{\perp}^2 \rangle)k^2$, where k is the gamma ray wave vector (from Goldanskii and Makarov 1968).

Although the Goldanskii-Karyagin effect was originally, and is still most commonly, observed for quadrupole split spectra (Goldanskii *et al.* 1962), it is also observable in magnetically split spectra (Cohen at al. 1966). The effect is to alter the intensity of lines 2 and 5 relative to the other lines in the sextet, just as occurs in magnetic texture. The latter effect is far more likely and separating the two contributions, if both are present, can be difficult.

1.6 Diffusional Broadening

The derivation of the f-value in section 1.1.1 assumed that the emitting or absorbing nucleus remained at its lattice site during the lifetime of the nuclear state. However, as one increases the temperature to near the melting point or nears a crystallographic phase transition, this may no longer be true. Diffusional effects may also be observed in glasses or materials with a high concentration of vacancies. Essentially one needs the atom to move a distance large compared to the gamma ray wavelength (0.086 nm for ^{57}Fe) in a time smaller than the nuclear lifetime. All iron interatomic distances will satisfy this

first criterion.

The original theory is due to Singwi and Sjölander (1960). In a solid, diffusion is best considered as a discontinuous jump of an atom from one lattice site to a neighbouring lattice site with a mean time of τ_D. Then the maximum expected line broadening should be $\Delta\Gamma = 2\hbar/\tau_D$ for diffusion parallel to the gamma ray beam and decreases to zero if it is perpendicular. There is no associated reduction in the f-value.

Atomic diffusional effects have been observed in many different materials. Examples are:

(i) line broadening due to diffusion in a viscous liquid: iron in glycerol (Bunbury *et al.* 1963),

(ii) line broadening due to diffusion in metals: iron in copper, gold, aluminium, titanium and yttrium (Knauer and Mullen 1968a, 1968b, Flinn 1980 and references therein)

(iii) collapse of the quadrupole splitting due to vacancy movement: AgCl:Fe^{2+} (Lindley and Debrunner 1966), wüstite, $Fe_{1-x}O$ (Greenwood and Howe 1972, Anand and Mullen1973) and Fe-C austenite (Lewis and Flinn 1968),

(iv) glass transition temperature: H_3PO_4:Fe + H_2O (Flinn *et al.* 1976)

In the case of wüstite, it was possible to change the number of oxygen vacancies at fixed temperature by controlling the oxygen pressure. Calculations of the expected collapse of the quadrupole splitting due to vacancy motion have been carried out by Dattagupta (1976). It is interesting to note that if it is the Mössbauer atom which moves, then in principle we should get narrowing of the hyperfine interaction (similar to motional narrowing in NMR) and a line broadening due to translational motion. Narrowing of the magnetic hyperfine interaction should also be observed, but most materials have their magnetic ordering temperature lower than the temperature at which diffusional effects become important.

Although the effects of atomic diffusion can be observed, they are relatively unlikely to be observed under most conditions. The above examples have all been carried out specifically to see if the effects are observable using Mössbauer spectroscopy rather than using it as a technique for studying diffusion. For further details see the reviews by Flinn (1980), Dattagupta (1983) and Kolk (1984).

Another form of diffusion is the macroscopic diffusion of nanometre scale particles where a Brownian motion type of diffusion takes place in a bounded region. A good example of this is shown by Plachinda *et al.* (1990) using 3-5 nm particles of ferric hydroxide precipitated in a polymer network. The observed displacements ranged from 10-60 pm which produced wings on the spectrum stretching out to 100 mm/s.

1.7 Mössbauer Spectroscopy in Mineralogy and Minerals Processing

Now that we have dealt with the most important theoretical bases of Mössbauer spectroscopy, we are in a position to consider how it can be applied to mineralogy and mineral processing. In our view, Mössbauer spectroscopy is not currently used as much as it should be in these areas. What are the objective reasons for and against its wider use?

1.7.1 Characteristics of Mössbauer Spectroscopy – Strengths and Weaknesses

Let us start by summarising the major characteristics of Mössbauer spectroscopy and their effects on the use of the technique. This is done in tabular form in Table 1.6. Most of these details have been put together as a result of many years of answering exploratory questions from prospective customers for contract Mössbauer analysis. Knowing the strengths and weaknesses of a proposed investigation is important regardless of whether you are working out if it is worth paying money to get it done or if you are trying to encourage a customer without setting too high an expectation.

We will leave it to the reader to select the parts of Table 1.6 which they regard as most useful to them. There will be further comments on the fitting and interpretation of spectra in chapter 3, together with a table of potential difficulties and some suggestions for overcoming them.

1.7.2 Characterization of New or Unknown Phases

Identification of any phase is done by applying a test for which the result will uniquely specify that phase, or a series of tests which, when taken together, uniquely specify that phase. Mössbauer spectroscopy is one of the spectroscopic techniques which may be used to fingerprint phases. In order to do this, banks of the data had to be built up on samples which had already been characterized by some other technique. As an example of the systematics which are built up from these data bases, Figure 1.14 shows how measurement of the isomer shift and quadrupole splitting can give a good idea of the valence and coordination of iron atoms.

For details of the data base kept by the Mössbauer Effect Data Center (MEDC), situated at the University of North Carolina at Asheville, NC, United States, see the bibliography at the end of the book.

If you are checking the parameters of your spectrum against the expected values for a known compound, this is relatively straightforward. However, in spite of the well-documented data, it is not a straightforward operation to identify the phase of your material purely from the parameters

unless you already have a good idea of what it is. Similarly, if you think that you have a new phase, it is not an easy task to check that the parameters do not satisfy some already known material, unless you can look up all the likely contenders individually.

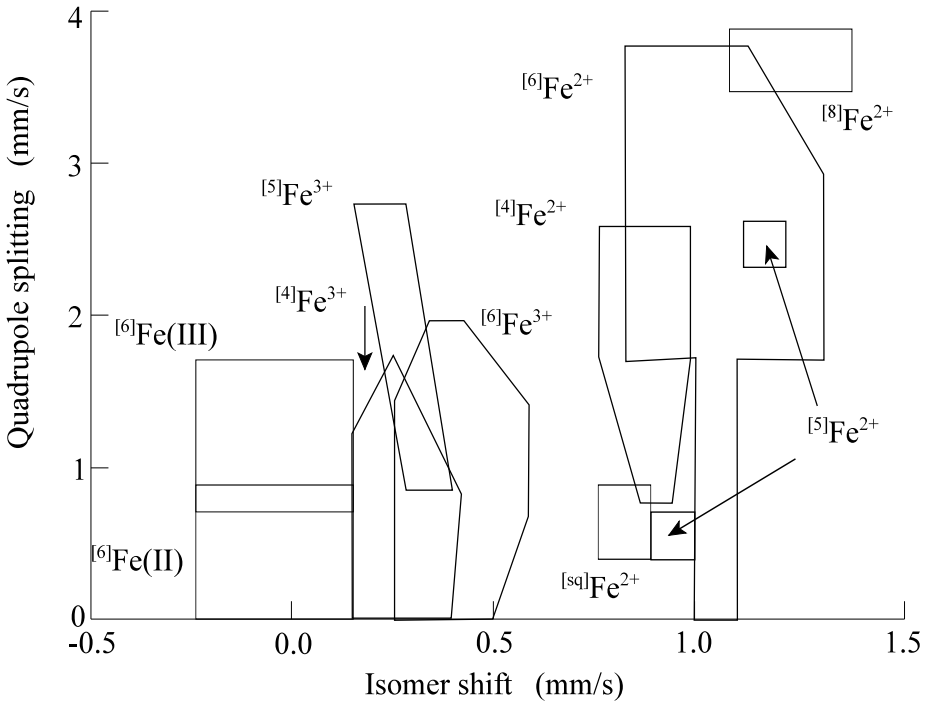

Figure 1.14. Allowed ^{57}Fe quadrupole splitting-isomer shift combinations for different valence states and coordination. The number in square brackets is the coordination number, with [6] indicating octahedral, [4] indicating tetrahedral and [sq] indicating square planar. High and low spin is indicated conventionally by the superscript valency or bracketed Roman numerals respectively. The isomer shift is referenced to α-Fe at room temperature.

1.7.3 Identification of Phases

When one thinks of phase identification, usually XRD is the first technique which comes to mind. XRD does not have the severe limitation on the number of elements to which it is sensitive and it is much quicker to take and, usually, to analyse. In short, if you can obtain your desired information from XRD, then do so. So what is the niche of Mössbauer spectroscopy when it comes to phase analysis? There are several.

The first niche is in poorly crystalline ferric oxides and oxyhydroxides

which frequently may not give an interpretable XRD spectrum. This may be because they are X-ray amorphous, in other words the coherence length is too short because of poor crystallinity or small particle size. It may be because they are a thin surface coating, possibly being formed in some natural or man-made process.

Table 1.6. Comparison of the advantages and disadvantages of some of the characteristics of Mössbauer spectroscopy in analysing iron-containing samples.

Characteristic	Advantage	Disadvantage
nuclide specific	insensitive to phases which do not contain the particular nuclide	limited range of elements which can be studied
competing phases		limited range of phases can be studied. Resolution varies depending on specific phases involved.
sample phase must be solid or frozen solution		eliminates investigations on liquids or gases
photon penetration ~10-100 mg/cm^2	reasonable size sample, may ensure representative of bulk	difficult to study microscopic samples
	no skin depth problems with metal samples	
typical lowest concentration ~0.2% Fe	not swamped with signals from insignificant iron impurities	limited sensitivity for studying impurities. Serious limitation for less abundant elements, *e.g.* ^{197}Au
parameters sensitive principally to nearest neighbour atoms	ability to characterize (fingerprint) phases	many phases have similar n.n. arrangements, *e.g.* Fe octahedrally coordinated to oxygens, so specificity not always adequate

good sample crystallinity not needed	relatively good spectra on poorly crystalline and glassy samples	
impurities	variable sensitivity, high in magnetically ordered samples, low if impurity is not coordinated to a significant percentage of Mössbauer atoms	
instrumentation	basic RT spectrometer cheap and relatively ageless	many investigations require better instrumentation for unambiguous interpretations, *e.g.* high and low (≤80 K) temperatures, large magnetic fields (>10T)
spectral fitting	in good cases, lineshape is known (Lorentzian) and fitting straightforward	in inhomogeneous samples, lineshape is not known
	good software packages now commercially available	can lose the science in the mathematics
		resolution may be inadequate for unambiguous fit
		magnetic relaxation can make spectrum very difficult to fit
		combined electric quadrupole and magnetic dipole interactions can make spectrum very difficult to fit, particularly for Fe^{2+}
interpretation of fitting and parameters	in good cases, straightforward	in many cases can be ambiguous - even experienced workers can make mistakes

	often possible for magnetically ordered phases, less often for paramagnetic phases	progression from fitted parameters to interpretations and phase determination not well documented. Strong reliance on experience
		not many minerals can be identified from Mössbauer spectroscopy alone because of the range of parameters due to compositional and crystallographic variations

The second niche is in the glasses and slags. With silica being a large component of most mineral bodies, glasses can be formed naturally as well as being common constituents of many mineral processing treatments.

A third niche is when there are several phases with similar XRD patterns, for example spinels. Sometimes their Mössbauer spectra may be better resolved.

A fourth niche in the gold processing area is the identification of gold species and "hidden gold" in ores or adsorbed onto activated carbon or polyurethane foam (Section 12.5).

Finally, any phase identification which relies on a single technique is going to fail sometimes. So looking for areas in which Mössbauer spectroscopy is "the best" is not the end of the story. Mössbauer spectroscopy is an important complementary technique to many of the more conventional ones and should be treated as such.

1.7.4 Quantitative Analysis

The area of the absorption line(s) from a phase is proportional to the amount of iron in that phase. If our sample has several phases, what we usually want to know is what is the proportion of each phase? So we measure the relative areas of the subspectra belonging to each phase. There are now two major steps to undertake in converting the area proportions to phase proportions and each has a difficulty associated with it.

The first is that the f-values of the different phases are likely to be, at least slightly, different. The f-values of mineral species have only been measured for a relatively small number of minerals and even then the f-value will decrease from the bulk value if the particle size is in the region of tens of nanometre or smaller. Methods of measuring the f-value are discussed in

section 3.4.

The second problem relates to the purity of the phase. Let us imagine that one of the phases is magnesioferrite, but instead of being pure it has a moderate (a few percent) aluminium impurity, so that it is $Mg(Fe_{1-x}Al_x)_2O_4$. If we have overcome the f-value problem successfully, then determining the proportion of total iron which is in the phase tells us how much magnesioferrite we have. We need a separate estimate of the aluminium impurity concentration in order to scale this up to the proportion of magnesium aluminoferrite. In this example, measurement of the decrease in the hyperfine field from the value for pure magnesioferrite should tell us the proportion of aluminium. However, in non-magnetically ordered minerals, it is a much more difficult task to estimate the impurity level from changes in the isomer shift or the quadrupole splitting, which depend on how different the bonding and ionic size are. An example of the dependence of the quadrupole splitting on composition in three solid solution spinels is shown in Figure1.15 (Vandenberghe and De Grave 1989). Similarly, Figure 1.16 shows the dependence of the hyperfine field and the isomer shift for another two sets of spinel solid solutions (Vandenberghe and De Grave 1989).

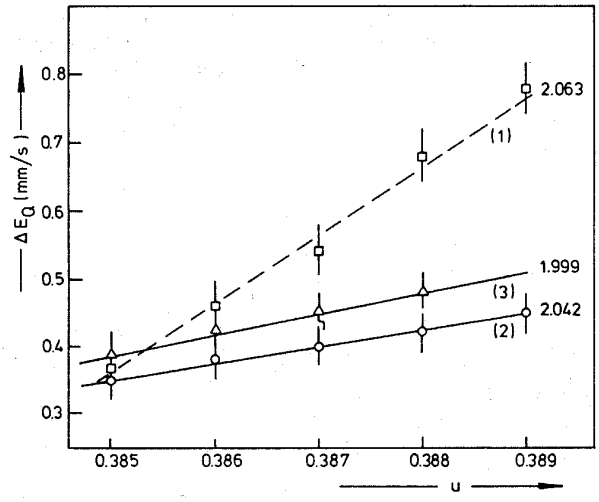

Figure 1.15. Dependence of the quadrupole splitting on the oxygen parameter, u, for three solid solution series: □ $Zn_{1-x}Cd_xFe_2O_4$, △$Mg_{1+x}Ti_xFe_{2(1-x)}O_4$ and ○ $Zn_{1+x}Sn_xFe_{2(1-x)}O4$ (from Vandenberghe and De Grave 1989).

These are physical problems relating to the specimen and there are quite a few other problems to be overcome in achieving valid fitting of the spectra. These include the effects of absorber thickness broadening, polarization effects

with single crystals and dealing with partially overlapping lines. These will be dealt with in chapter 3.

These statements should not be interpreted as implying that quantitative phase measurements with Mössbauer spectroscopy are not possible or indeed are any worse than competing techniques. For example, quantitative phase determination from the intensity of XRD lines has a similar set of difficulties with different Debye-Waller factors for the phases, the effect on line intensities of any texture or nanoscale particles and the variable effect of impurities on the line positions which is principally dependent on the relative ionic radii.

Mössbauer spectroscopy is a good complementary way of building up or checking the accuracy of phase diagrams of iron-containing compounds. This is just an extension of the phase analysis and is straightforward if the phases have definite stoichiometries. If this is not the case, then the variation in some hyperfine parameter with composition needs to be known. It is also important that the f-values are known before converting relative areas into proportions of iron in the phases.

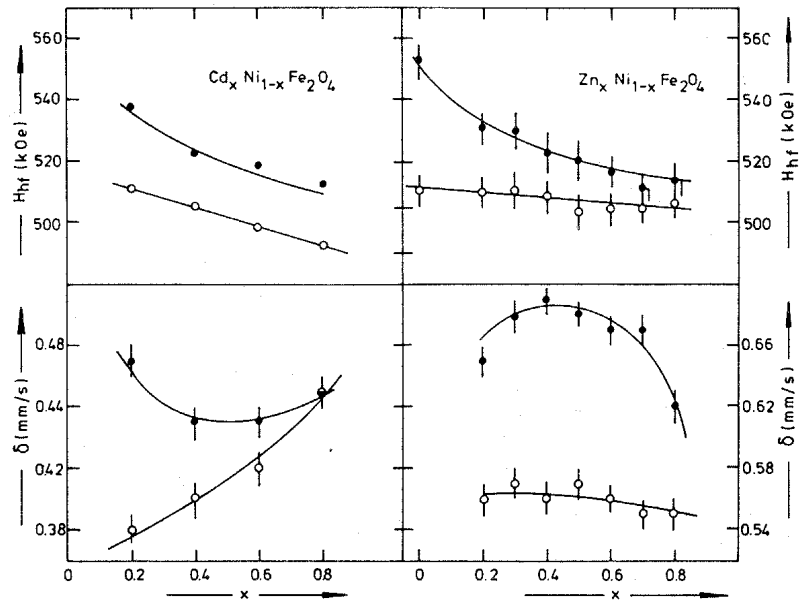

Figure 1.16. Hyperfine fields (H_{hf}) and isomer shifts (δ) as a function of composition, x, for the A-sites (○) and B-sites (●) of the solid solution series $Cd_xNi_{1-x}Fe_2O_4$ and $Zn_xNi_{1-x}Fe_2O_4$ (from Vandenberghe and de Grave 1989).

1.7.5 Crystallographic Transformations

Because of its sensitivity to nearest neighbour coordination, Mössbauer spectroscopy is very well suited to studying crystallographic phase transformations. Since these usually also involve a change in symmetry and volume, there are usually discontinuous changes in the isomer shift and quadrupole splitting at the transition temperature. If the transition is mediated by a soft phonon mode, then there will also be a change in the overall area of the spectrum as it approaches the transition from above. A comprehensive review of dynamic effects has been given by Kolk (1984).

1.7.6 Chemical Transformations and Bioprocesses

Since Mössbauer spectroscopy is capable of identifying phases, it is clear that by comparing successive spectra it must be possible to follow the course of chemical processes, natural or man-made, which convert one phase into another. Examples will be given later, particularly in Chapters 8 and 10 - 12.

Because of the time needed for data collection, spectra are usually taken by removing samples after particular intervals of time during a process. However, there have been a small number of cases where spectra were taken during a dynamic process, with a new spectrum being started at regular time intervals, say every 10-15 minutes.

Some mineral processes are mitigated by the presence of biological agents and Mössbauer spectroscopy is a convenient way of following the changes which are induced. If the changes are relatively fast so that a measurable change will occur during the time of acquisition of a spectrum, then the process can usually be stopped by doing the spectrum at low temperature. Even reducing it below the ice point is usually sufficient, although many groups find it more convenient to measure at temperatures in the liquid nitrogen region.

Some of the processes which can be followed are changes in soil composition (Section 7.1), green rusts (Section 9.1), the oxidation of pyritic ores by the *Thiobacillus ferrooxidans* and related species and the ensuing systems of acid mine drainage (Sections 8.2 and 9.4), and the preferential attack of bacteria on some mineral species rather than others (Section 12.5.2).

1.7.7 Radiation Damage

The effects of very severe radiation damage can be observed, for example after sustained neutron or electron irradiation. As we saw in Table 1.6, this is because of the relatively substantial proportion of iron atoms which need to be affected (~1-5%) in order for them to be conveniently studied. This proportion is much higher than needed by techniques such as EPR and means that Mössbauer spectroscopy cannot usually be applied for studying naturally

irradiated mineral samples.

An example of a successful study was to gadolinite, $R_2FeBe_2Si_2O_{10}$, (R = rare earth or yttrium) which had approximately 1wt-% of U + Th incorporated in the structure (Malczewski 2002). The radiation damage caused by the α-decays had caused a complete transformation from the original crystalline state to an amorphous state (metamictization). Malczewski (2002) followed the recrystallization of such a specimen by taking spectra on quenched samples heated under argon at temperatures between 873 and 1473 K. The spectrum of the initial sample showed a broad distribution of ferrous doublets, giving an asymmetric lineshape. The width of this distribution narrowed considerably with heating up to 1073 K, accompanied by recovery of a sharp X-ray diffraction pattern in place of the initial featureless one from the glass. Further heating produced only a small reduction in the quadrupole splitting in the doublet, which had now reversed its asymmetry.

1.8 Summary

A considerable amount of information has been included in this chapter, possibly an almost overwhelming amount for a new worker. The first major theme is the origin of the electron-nucleus (hyperfine) interactions, namely the isomer shift, the electric quadrupole interaction and the magnetic dipole interaction, which determine the shifts, splittings, and line intensities in the observed spectrum. The second theme covers the relevant electronic properties such as the bonding strength, symmetry and valency and the magnetic properties, which are all characteristic in identifying a material. A complication to the magnetism story is the possible occurrence of magnetic relaxation, which has two main forms. The first type is fast relaxation, which is common in fine particle and poorly crystalline iron oxides, and which can give a spectrum without magnetic splitting even though the sample is magnetically ordered. The second type is slow paramagnetic relaxation, which can occur in samples which are very dilute in iron, and give magnetically split spectra even though the sample is not magnetically ordered. The experimenter needs to be able to recognize the occurrence of either of these effects in the spectrum. The systematics used in phase identification and quantitative phase analysis are outlined, the latter being expanded in Chapter 3. Finally, Table 1.6 provides a summary of the strengths and weaknesses of Mössbauer spectroscopy in mineralogical analysis, but also applicable to analysis in any area.